Appendix H.

PFW dispersion modelling study (RPS 2017a)

RPS

ConocoPhillips Barossa Project

Produced Formation Water Dispersion Modelling

Prepared by:

RPS

Suite E1, Level 4
140 Bundall Rd
Bundall, QLD 4217

T: +61 7 5574 1112
F: +61 8 9211 1122
E: szigic@pasa.com.au

Client Manager: Dr Sasha Zigic
Report Number: MAQ0540J.000
Version / Date: Rev1/14 March 2017

Prepared for:

CONOCOPHILLIPS AUSTRALIA

Dr Brenton Chatfield
53 Ord Street
West Perth WA 6005

Mail: PO Box 1102
        West Perth WA 6872

T: +61 8 6363 2666
E: Brenton.S.Chatfield@conocophillips.com
W: www.conocophillips.com.au

Document Status

Version	Purpose of Document	Original	Review	Review Date
DraftA	*Issued for client review*	Dr Ryan Dunn	Dr Sasha Zigic	28/2/2017
Rev 0	*Issued for client review*	Dr Ryan Dunn	Dr Sasha Zigic	28/2/2017
Rev 1	Issued to client		Dr Sasha Zigic	14/3/2017

Approval for Issue

Name	Signature	Date
Dr Sasha Zigic	*S. Zigic*	14/3/2017

DISCLAIMER:

This report has been issued to the client under the agreed schedule and budgetary requirements and contains confidential information that is intended only for use by the client and is not for public circulation, publication, nor any third party use without the approval of the client.

Readers should understand that modelling is predictive in nature and while this report is based on information from sources that RPS considers reliable, the accuracy and completeness of said information cannot be guaranteed. Therefore, RPS, its directors, and employees accept no liability for the result of any action taken or not taken on the basis of the information given in this report, nor for any negligent misstatements, errors, and omissions. This report was compiled with consideration for the specified client's objectives, situation, and needs. Those acting upon such information without first consulting RPS, do so entirely at their own risk.

Contents

Tables

Figures

1.0   Introduction

1.1   Project background

ConocoPhillips Australia Exploration Proprietary (Pty) Limited (Ltd.) (ConocoPhillips), as proponent on behalf of the current and future co-venturers, is proposing to develop natural gas resources in the Timor Sea into high quality products in a safe, reliable and environmentally responsible manner. The Barossa Area Development (herein referred to as the "project") is located in Commonwealth waters within the Bonaparte Basin, offshore northern Australia, and is approximately 300 kilometres (km) north of Darwin, Northern Territory (NT).

The development concept of the gas resource includes a floating production storage and offloading (FPSO) facility and a gas export pipeline that are located in Commonwealth jurisdictional waters. The FPSO facility will be the central processing facility to stabilise, store and offload condensate, and to treat, condition and export gas. The extracted lean dry gas will be exported through a new gas export pipeline that will tie into the existing Bayu-Undan to Darwin gas export pipeline. The lean dry gas will then be liquefied for export at the existing ConocoPhillips operated Darwin Liquefied Natural Gas facility at Wickham Point, NT.

Produced formation water (PFW) will be generated during the project and will be discharged into the open ocean. The PFW stream is generally characterised as having a naturally high temperature due to exposure to geothermal heat in the reservoir and may contain a mixture of constituents including dissolved and dispersed hydrocarbons at levels exceeding the receiving marine waters.

The volumes of PFW generated from the hydrocarbon reservoirs will vary over the life of the field. The volumes of PFW tend to be lowest at the start of production and peak towards to end of each field's lifecycle.

To assess the change in temperature and rate of mixing of the residual condensate in the PFW stream from the FPSO facility, ConocoPhillips commissioned RPS to undertake a dispersion modelling study for the two flow rates (minimum of 1,590 m^3/d and maximum of 3,260 m^3/d). The coordinate of the indicative release location is presented in Table 1 and graphically in Figure 1. The purpose of the modelling was to assist in understanding the potential area that may be influenced by the routine discharge of PFW based on the engineering information available in the early stage of the project design phase.

The potential area that may be influenced by the PFW discharge stream was assessed for three distinct seasons; (i) summer (December to the following February), (ii) the transitional periods (March and September to November) and (iii) winter (April to August). This approach assists with identifying the environmental values and sensitivities that would be at risk of exposure on a seasonal basis.

The closest environmental values and sensitivities to the modelled release location are submerged shoals and banks including Lynedoch Bank (70 km to the south-east), Evans Shoal (64 km to the west) and Tassie Shoal (74 km to the south-west).

Table 1 Barossa offshore development area PFW dispersion modelling study release location

Release location	Latitude	Longitude	Water depth (mLAT)
Barossa offshore development area release location	9° 52' 35.8" S	130° 11' 8.4" E	~230
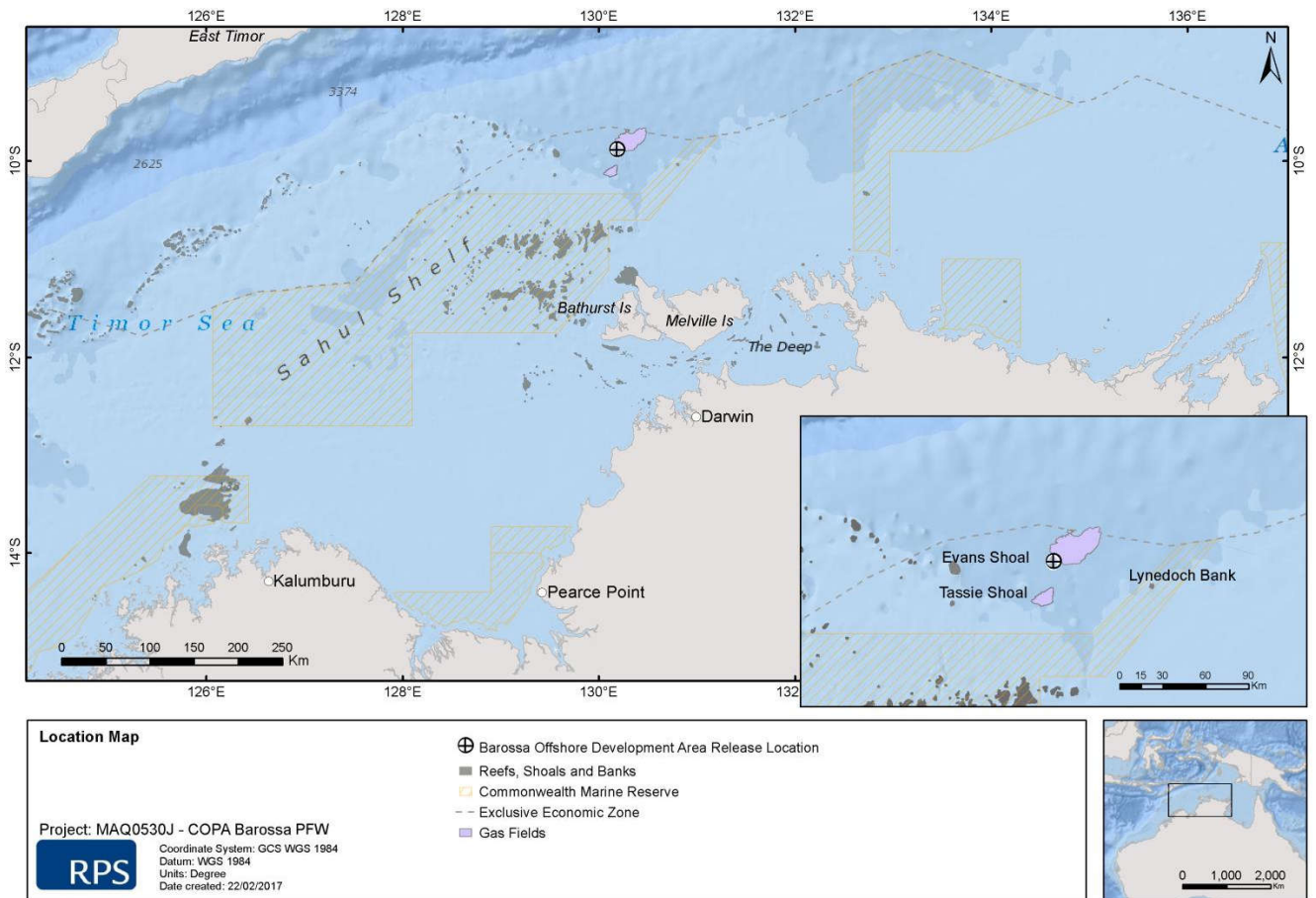
Figure 1 Map of the Barossa offshore development area PFW modelling study release location.

2.0   Dispersion modelling

The physical mixing of the PFW stream can be separated into two distinct zones; near-field and far-field.

The near-field zone is defined by the region where the levels of mixing and dilution are controlled by the plume's initial jet momentum and the buoyancy flux, resulting from the density difference. When the plume encounters a boundary such as the water surface, seabed or density stratification layer, the near-field mixing is complete and the far-field mixing begins. During the far-field phase, the plume is transported and mixed by the ambient currents.

Therefore, to accurately determine the dilution and the mixing zone of the PFW water stream, the effect of near-field mixing needs to be considered first, followed by an investigation of the far-field mixing. Section 2.1 and Section 2.2 describe the near-field and far-field dispersion model. The physical mixing of the PFW water stream can be separated into two distinct zones; near-field and far-field.

2.1   Near-field model

2.1.1   Description

The near-field mixing of the PFW water discharge stream was predicted using the fully three-dimensional flow model, Updated Merge (UM3). The UM3 model is used for simulating single and multi-port submerged

discharges and is part of the Visual Plumes suite of models maintained by the United States Environmental Protection Agency (Frick et al. 2003).

The UM3 model has been extensively tested for various discharges and found to predict the observed dilutions more accurately (Roberts and Tian 2004) than other near-field models (e.g. RSB or CORMIX).

In this Lagrangian model, the equations for conservation of mass, momentum, and energy are solved at each time-step, giving the dilution along the plume trajectory. To determine the growth of each element, UM3 uses the shear (or Taylor) entrainment hypothesis and the projected-area-entrainment hypothesis. The flows begin as round buoyant jets issuing from one side of the diffuser and can merge to a plane buoyant jet (Carvalho et al. 2002). Model output consists of plume characteristics, including centerline dilution, rise-rate, width, centreline height and diameter of the plume. Dilution is reported as the "effective dilution", which is the ratio of the initial concentration to the concentration of the plume at a given point, following Baumgartner et al. (1994).

2.1.2   Model setup

The PFW discharge characteristics are summarised in Table 2. The PFW discharge was modelled 10 m below the water surface through a single outlet, and was anticipated to have a salinity, temperature and initial oil in water (OIW) concentration of 15 parts per thousand (ppt), 60°C and 30 milligrams per litre (mg/L), respectively.

The volumes of PFW generated from the project will vary over the life of the field. In general, PFW volumes are lowest at the start of production and peak towards to end of each field's lifecycle. Based on the engineering definition available at the time of commissioning the dispersion modelling study, the minimum and maximum (peak) volumes are estimated at 1,590 m^3/d and 3,260 m^3/d, respectively.

Additional input data used to setup the near-field model included range of current speeds, water temperature and salinity as a function of depth. Defining the water temperature and salinity is important to correctly replicate the buoyancy of the plume. The buoyancy dynamics in this case will be dominated by the temperature and salinity differences between the PFW plume and receiving waters. Table 3 presents the measured water temperature and salinity data collected by Fugro (2015) as part of the Barossa marine studies program. The minimum water temperature at 30 m below mean sea level (BMSL) was used as it represents the most conservative conditions considering water temperature varies with depth and would be warmer at the surface in comparison to temperatures at 30 m.

Table 4 presents the 5th, 50th and 95th percentiles of current speeds, which reflect contrasting dilution and advection cases:

- 5th percentile current speed: weak currents, low dilution and slow advection
- 50th percentile (median): medium current speed, moderate dilution and advection
- 95th percentile current speed: strong currents, high dilution and rapid advection to nearby areas.

The 5th percentile, 50th percentile (median) and 95th percentile values are referenced as weak, medium and strong current speeds, respectively.

Table 2 PFW discharge and pipe configuration characteristics summary

Parameter	Value/design
Flow rate (m^3/d)	Minimum flow rate: 1,590 Maximum flow rate: 3,260
Outlet pipe internal diameter (m)	0.310

Parameter	Value/design
Pipe orientation	Vertically downward
Depth of pipe below sea surface (m)	10
Discharge salinity (ppt)	15
Discharge water temperature (°C)	60
Initial OIW concentration (mg/L; ppm)	30

Table 3 Water temperature and salinity model inputs

Parameter	Season		
	Summer	Transitional	Winter
Ambient minimum water temperature (°C) (30 m BMSL)	25.4	24.7	26.3
Ambient mean salinity (Practical Salinity Units (PSU)) (30 m BMSL)	34.1	33.6	33.6

Table 4 Seasonal ambient percentile current speeds, strength and predominant direction as a function of water depth at the release location

Depth below the water surface (m)	Parameter	Reporting current strength	Season					
			Summer		Transitional		Winter	
			Speed (m/s)	Predominant direction	Speed (m/s)	Predominant direction	Speed (m/s)	Predominant direction
0	5th percentile	Weak	0.04	East	0.05	West-south-west	0.03	South-west
	50th percentile	Medium	0.11		0.14		0.11	
	95th percentile	Strong	0.27		0.29		0.27	
10	5th percentile	Weak	0.03	East	0.03	South-west	0.04	South-west
	50th percentile	Medium	0.09		0.12		0.12	
	95th percentile	Strong	0.23		0.26		0.25	
20	5th percentile	Weak	0.03	East-south-east	0.03	South-west	0.03	South-west
	50th percentile	Medium	0.08		0.11		0.12	
	95th percentile	Strong	0.20		0.24		0.24	

2.2   Far-field model

2.2.1   Description

The far-field modelling expands on the near-field model predictions as it also takes into account the time-varying nature of currents, together with the potential for recirculation of the plume back to the release location. In the latter case near-field concentrations can be increased due to the discharge plume mixing with the remnant plume from an earlier time.

The three-dimensional plume behaviour model, MUDMAP, was used to simulate the far-field mixing and dispersion of the OIW within the PFW plume. MUDMAP is an industry standard computerised modelling system, which has been applied throughout the world to predict the dispersion of sediment (cuttings and muds) and liquid (produced water) discharges since 1994 (Spaulding 1994). The model is a development of the Offshore Operators Committee (OOC) model and like the OOC model calculates the fates of discharges through three known distinct integrated stages (Koh and Chang 1973; Khondaker 2000; Brandsma and Sauer Jr 1983a, 1983b).

The PFW release is represented by placing a fixed number of "particles" at the release location on each time-step. These particles are moved on each subsequent time-step according to the horizontal and vertical components from the hydrodynamic model. The plume spread is dependent on the horizontal and vertical mixing coefficients.

The MUDMAP system is based on a conservative tracer (no reaction or decay), constituting a "worst case" scenario, to examine the mixing and dilution of effluent plumes. The concentration distribution of the constituent in water is estimated using a counting grid. The number of particles in a grid square over a depth interval from the water surface down to a specified depth is counted, giving the mass of the constituent in a known volume, and therefore concentration.

The system has been extensively validated and applied for discharge operations in Australian waters (e.g. Burns et. al. 1999; King and McAllister 1997, 1998).

2.2.2   Model setup

The MUDMAP model simulated the discharge into a time-varying current field with the initial dilution set by the near-field results described in Section 3.1.

The two PFW flow rates were modelled as a constant discharge for each month during 2010, 2012 and 2014. Once the results were complete, they were reported on a combined seasonal basis: (i) summer (December to the following February); (ii) the transitional (March, April, September to November) and (iii) winter (May to August).

MUDMAP uses a three-dimensional grid to represent the water depth and bathymetric profiles of the study area. Due to the rapid mixing and small-scale influences of the discharge, it was necessary to use a very fine grid with a resolution of 10 m x 10 m to track the movement and fate of the plume. The extent of the grid region measured 10 km (longitude or x-axis) x 10 km (latitude or y-axis). It is important to note, that the 10 m grid cell sizes were selected following extensive sensitivity testing in order to achieve similar dilution rates at the end of the near-field mixing.

Table 5 presents a summary of the far-field model parameters used to simulate the PFW discharges during the three seasons and two flow rates.

Spatially constant, conservative horizontal and vertical dispersion coefficients were used to control the exchange of the PFW in the horizontal and vertical directions respectively. The coefficients were selected following extensive sensitivity testing in order to recreate similar plume characteristics and dilutions at the end of the near-field mixing.

Table 5 Summary of the far-field PFW model inputs

Parameter	Value/design
Years simulated	• 2010 (La Niña conditions) • 2012 (neutral/mixed) • 2014 (El Niño conditions)
Seasons (months simulated and reported)	• Summer (December, January, February) • Transitional periods (March, April, September to November) • Winter (May to August)
Total months modelled and analysed per flow rate	36
Flow rate (m³/d)	Minimum flow rate: 1,590 Maximum flow rate: 3,260
Discharge type	Continuous
Period of discharge (days)	Entire month
PFW discharge temperature (°C)	60
PFW discharge salinity (ppt)	15
Initial OIW concentration (mg/L; ppm)	30

2.3 Interannual variability

The region is strongly affected by the strength of the Indonesian Throughflow, which fluctuates from one year to the next due to the exchange between the Pacific and Indian Oceans. Therefore, in order to examine the potential range of variability, the Southern Oscillation Index (SOI) data sourced from the Australian Bureau of Meteorology was used to identify interannual trends for the last 10 years (2005–2014). The SOI broadly defines neutral, El Niño (sustained negative values of the SOI below −8 often indicate El Niño episodes) and La Niña (sustained positive values of the SOI above +8 are typical of La Niña episodes) conditions based on differences in the surface air-pressure between Tahiti on the eastern side of the Pacific Ocean and Darwin (Australia), on the western side (Rasmusson and Wallace 1983, Philander 1990). El Niño episodes are usually accompanied by sustained warming of the central and eastern tropical Pacific Ocean and a decrease in the strength of the Pacific trade winds. La Niña episodes are usually associated with converse trends (i.e. increase in strength of the Pacific trade winds).

Figure 2 shows the SOI monthly values and Figure 3 shows the surface ocean current roses for the period 2004–2013 at the proposed release location. Each current rose diagram provides an understanding of the speed, frequency and direction of currents, over the given year:

▪ Current speed – speed is divided into segments of different colour, ranging from 0 to greater than 1 m/s. Speed intervals of 0.2 m/s are used. The length of each coloured segment is relative to the proportion of currents flowing within the corresponding speed and direction;

▪ Frequency – each of the rings on the diagram corresponds to a percentage (proportion) of time that currents were flowing in a certain direction at a given speed;

▪ Direction – each diagram shows currents flowing towards particular directions, with north at the top of the diagram.

Based on the combination of the SOI assessment and surface ocean currents, 2010 was selected as a representative La Niña year, 2012 was selected as a representative neutral year, and 2014 was selected as an El Niño year.
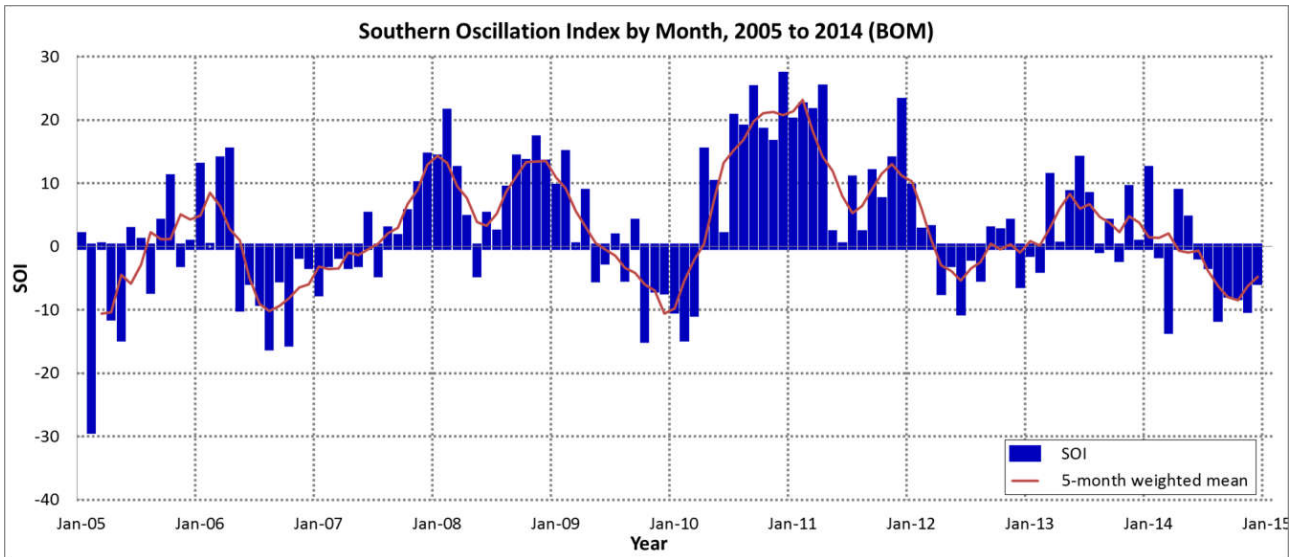
Figure 2 Monthly values of the SOI 2005-2014. Sustained positive values indicate La Niña conditions, while sustained negative values indicate El Niño conditions (Data sourced from Australian Bureau of Meteorology 2015).

RPS Data Set Analysis

Current Speed (m/s) and Direction Rose (All Records)

Longitude = 130.19°E, Latitude = 9.88°S
Analysis Period: 01-Jan-2005 to 31-Dec-2014

Color Key [Current Speed(m/s)] :

0 - 0.01 | 0.01 - 0.1 | 0.1 - 0.2 | 0.2 - 0.3 | 0.3 - 0.4 | 0.4 - 0.5 | 0.5 - 0.6 | 0.6 - 0.7 | 0.7 - 0.8 | 0.8 - 0.9 | 0.9 - 1
*Calm defined as < 0.01
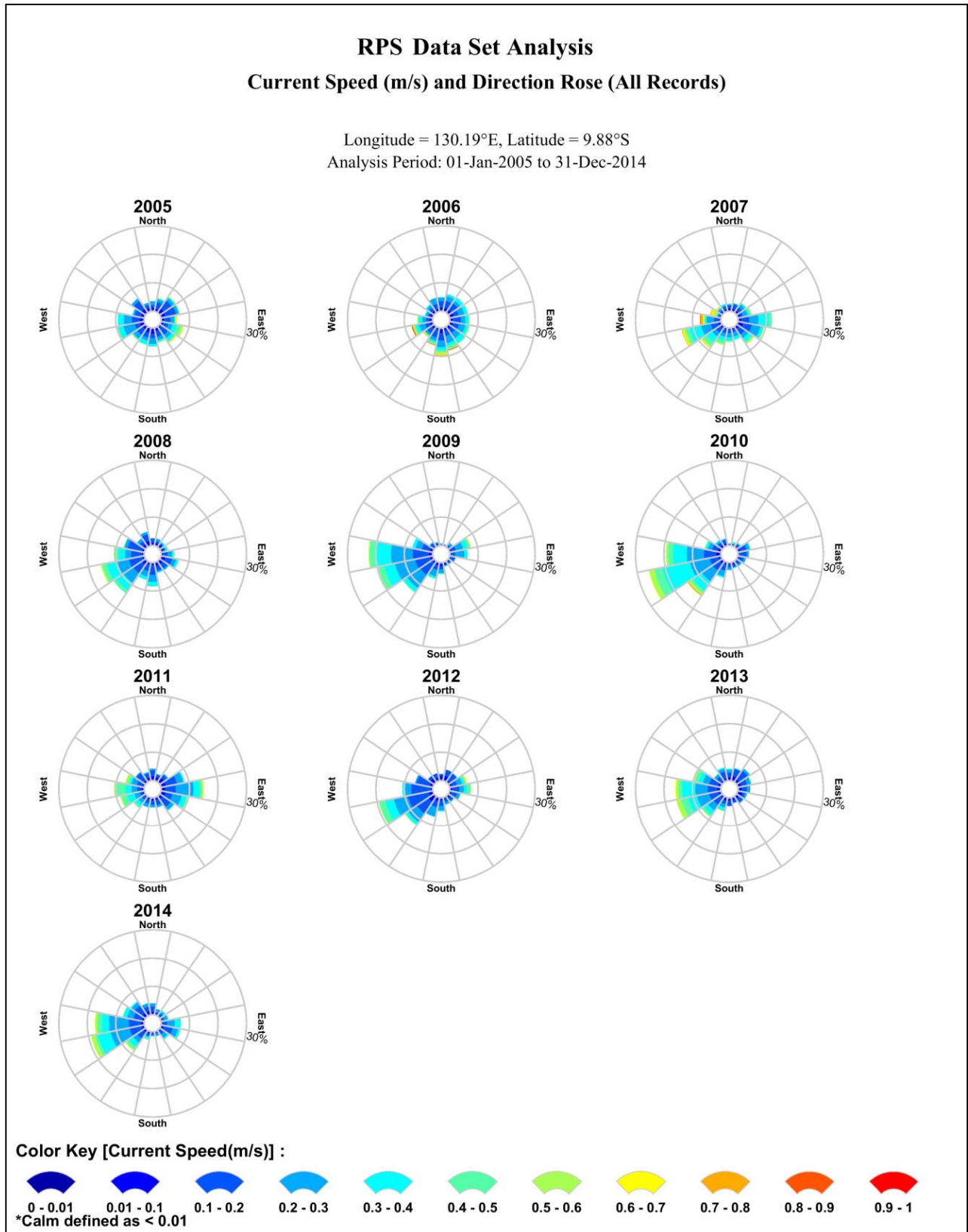
Figure 3 Annual surface ocean current rose plots within the Barossa offshore development area. Derived from analysis of HYCOM ocean data for the years 2005–2014. The colour key shows the current speed (m/s), the compass shows the direction and the length of the wedge gives the percentage of the record for a particular speed and direction combination.

2.4   Development of regional current data

The project is located within the influence of the Indonesian Throughflow, a large scale current system characterised as a series of migrating gyres and connecting jets that are steered by the continental shelf. This results in sporadic deep ocean events causing surface currents to exceed 1.5 m/s (approximately 3 knots).

While the ocean currents generally flow toward the southwest, year-round, the internal gyres generate local currents in any direction. As these gyres migrate through the area, large spatial variations in the speed and direction of currents will occur at a given location over time.

The influence of tidal currents is generally weaker in the deeper waters and greatest surrounding regional reefs and islands. Therefore, it was critical to include the influence of both types of currents (ocean and tides) to rigorously understand the likely discharge characteristics in the project's area of influence.

A detailed description of the tidal and ocean current data inputted into the model is provided below.

2.4.1   Tidal currents

The tidal circulation was generated using RPS's advanced ocean/coastal model, HYDROMAP. The HYDROMAP model has been thoroughly tested and verified through field measurements throughout the world over the past 26 years (Isaji and Spaulding 1984; Isaji et al. 2001; Zigic et al. 2003). In addition, HYDROMAP tidal current data has been used as input to forecast (in the future) and hindcast (in the past) condensate spills in Australian waters and forms part of the Australian National Oil Spill Emergency Response System operated by the Australian Maritime Safety Authority (AMSA).

HYDROMAP employs a sophisticated sub-gridding strategy, which supports up to six levels of spatial resolution, halving the grid cell size as each level of resolution is employed. The sub-gridding allows for higher resolution of currents within areas of greater bathymetric and coastline complexity, and/or of particular interest to a study.

The numerical solution methodology follows that of Davies (1977a, 1977b) with further developments for model efficiency by Owen (1980) and Gordon (1982). A more detailed presentation of the model can be found in Isaji and Spaulding (1984), Isaji et al. (2001) and Owen (1980).

1.1.1.1   Tidal grid setup

The HYDROMAP tidal grid was established over a domain that extended approximately 2,400 km (east–west) by 1,575 km (north–south) (Figure 4). Computational cells were square, with sizes varying from 8 km in the open waters down to 1 km in some areas, to more accurately resolve flows along the coastline, around islands and reefs, and over more complex bathymetry (Figure 5).

Bathymetry used in the model was obtained from multiple sources (Figure 6). This included bathymetry data sourced from the Geoscience Australia database and commercially available digitised navigation charts.
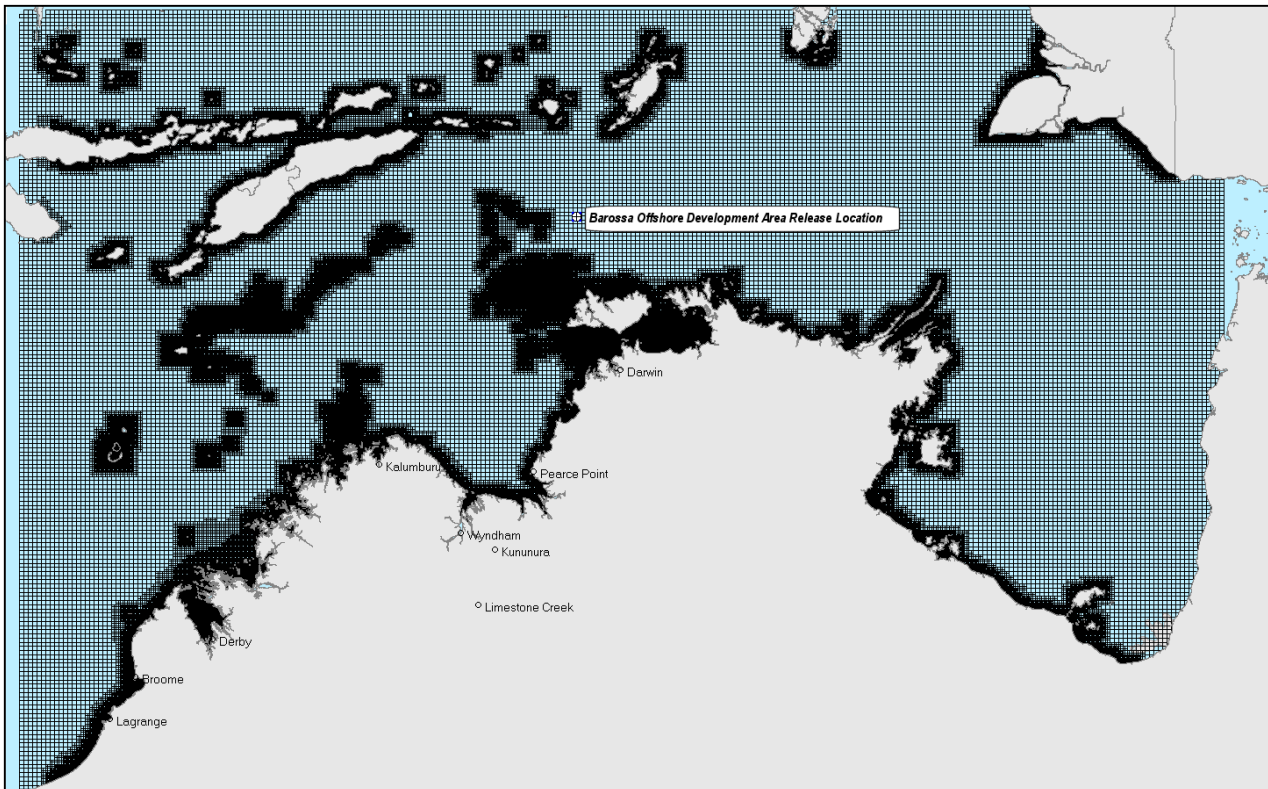
Figure 4 Map showing the extent of the tidal model grid. Note, darker regions indicate higher grid resolution.
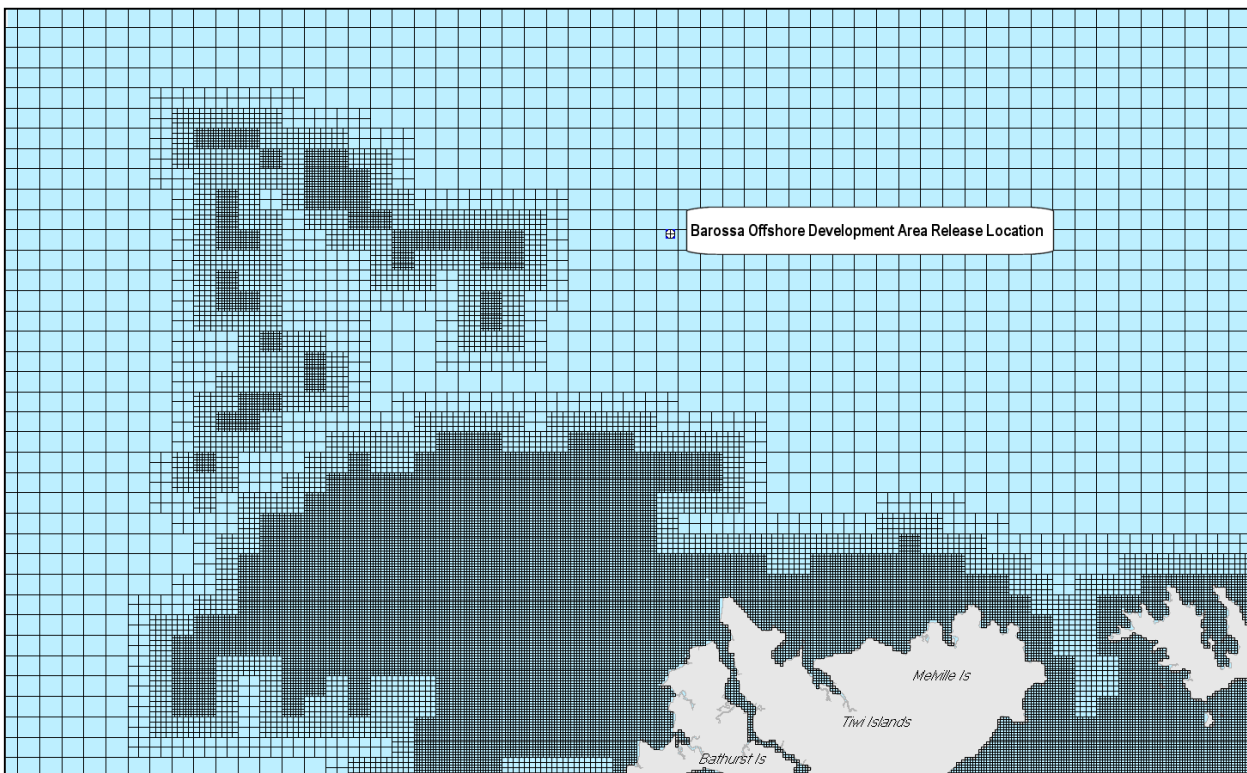
Figure 5 Zoomed in map showing the tidal model grid), illustrating the resolution sub-gridding in complex areas (e.g. islands, banks, shoals or reefs)
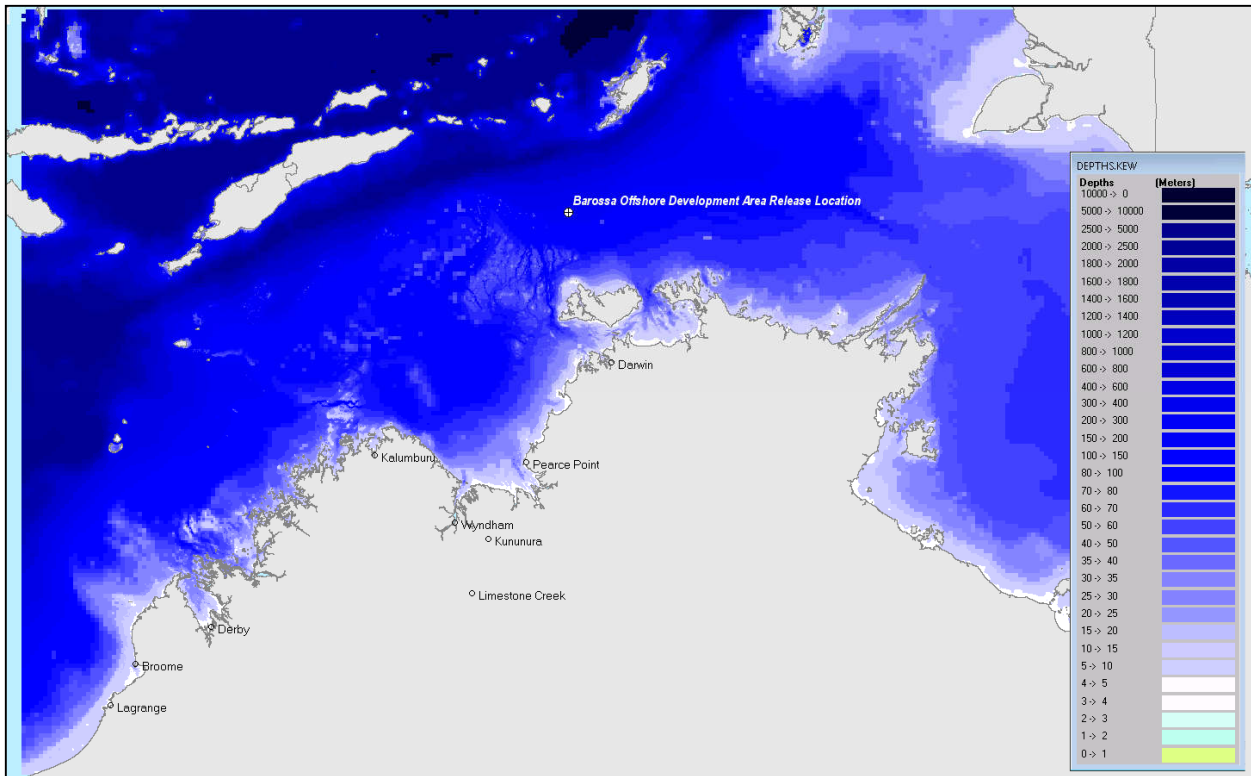
Figure 6 Map showing the bathymetry of the tidal model grid

1.1.1.2   Tidal data

The ocean boundary data for the regional model was obtained from satellite measured altimetry data (TOPEX/Poseidon 7.2) which provided estimates of the eight dominant tidal constituents at a horizontal scale of approximately 0.25 degrees. Using the tidal data, surface heights were firstly calculated along the open boundaries, at each time step in the model.

The Topex-Poseidon satellite data is produced and quality controlled by the National Aeronautics and Space Administration (NASA). The satellites, equipped with two highly accurate altimeters that are capable of taking sea level measurements to an accuracy of less than 5 cm, measured oceanic surface elevations (and the resultant tides) for over 13 years (1992–2005; see Fu et al., 1994; NASA/Jet Propulsion Laboratory 2013a; 2013b). In total these satellites carried out 62,000 orbits of the planet. The Topex-Poseidon tidal data has been widely used amongst the oceanographic community, being the subject of more than 2,100 research publications (e.g. Andersen 1995, Ludicone et al. 1998, Matsumoto et al. 2000, Kostianoy et al. 2003, Yaremchuk and Tangdong 2004, Qiu and Chen 2010). As such the Topex/Poseidon tidal data is considered accurate for this study.

2.4.2   Ocean currents

Data describing the flow of ocean currents was obtained from the Hybrid Coordinate Ocean Model (HYCOM) (see Chassignet et al. 2007, 2009), which is operated by the HYCOM Consortium, sponsored by the Global Ocean Data Assimilation Experiment (GODAE). HYCOM is a data-assimilative, three-dimensional ocean model that is run as a hindcast, assimilating time-varying observations of sea surface height, sea surface temperature and in-situ temperature and salinity measurements (Chassignet et al. 2009). The HYCOM predictions for drift currents are produced at a horizontal spatial resolution of approximately 8.25 km (1/12th of a degree) over the region, at a frequency of once per day. HYCOM uses isopycnal layers in the open, stratified ocean, but uses the

layered continuity equation to make a dynamically smooth transition to a terrain following coordinate in shallow coastal regions, and to zlevel coordinates in the mixed layer and/or unstratified seas.

For this modelling study, the HYCOM hindcast currents were obtained for the years 2010 to 2014 (inclusive). Figure 7 shows the seasonal surface current roses distributions adjacent to the release location by combining 2010, 2012 and 2014. The data shows that the surface current speeds and directions varied between seasons. In general, during transitional conditions (March, April and September to November) currents were shown to have the strongest average speed (average speed of 0.15 m/s with a maximum of 0.39 m/s) and tended to flow to the west-southwest. During summer (December to February) and winter (May to August) conditions the current flow was more variable though mostly toward the east and west, respectively. The average and maximum speeds during summer was 0.11 m/s and 0.41 m/s, respectively. During winter the average was 0.13 m/s and 0.47 m/s as the maximum.
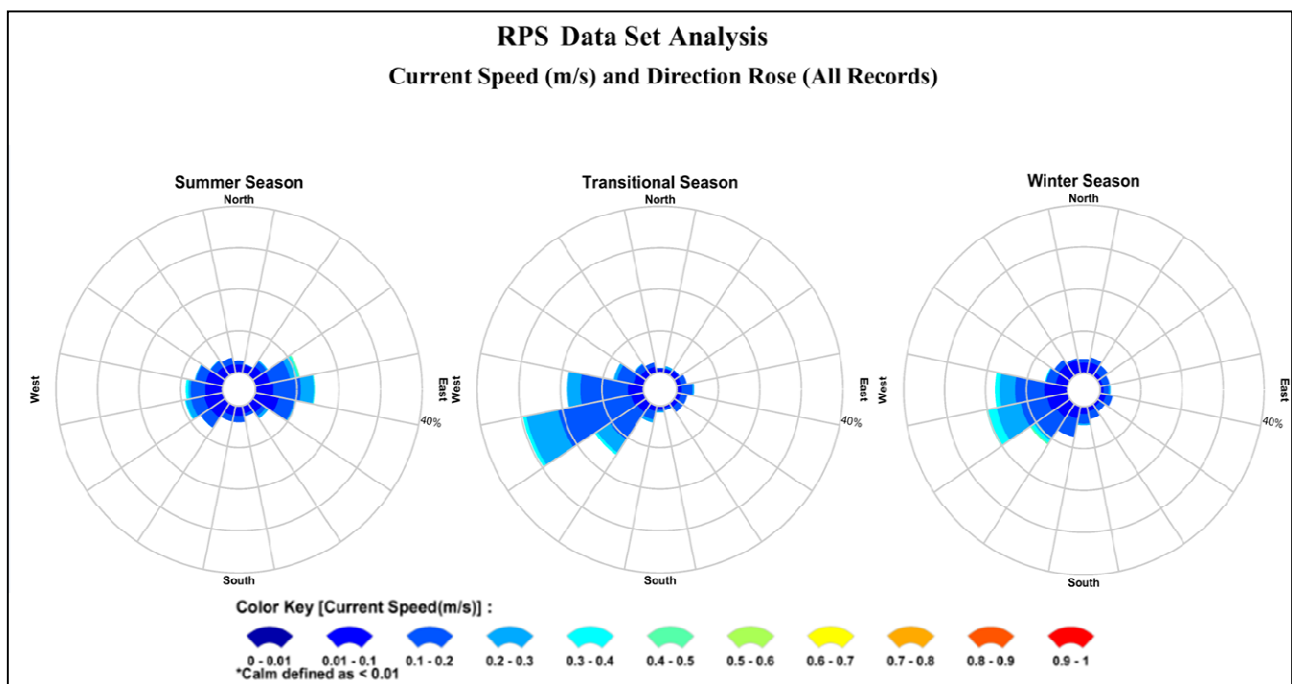
Figure 7 Seasonal surface current rose plots adjacent to the release location. Data was derived from the HYCOM ocean currents for years, 2010, 2012 and 2014. The colour key shows the current magnitude (m/s), the compass direction provides the current direction flowing TOWARDS and the length of the wedge gives the percentage of the record for a particular speed and direction combination.

Figure 8 shows example screenshots of the predicted HYCOM ocean currents during summer and winter conditions. The colours of the arrows indicate current speed (m/s).

In addition, Figure 9 to Figure 11 show the monthly surface current rose plots adjacent to the release location for 2010, 2012 and 2014, respectively. The data is derived by combining the ocean currents and tidal currents.
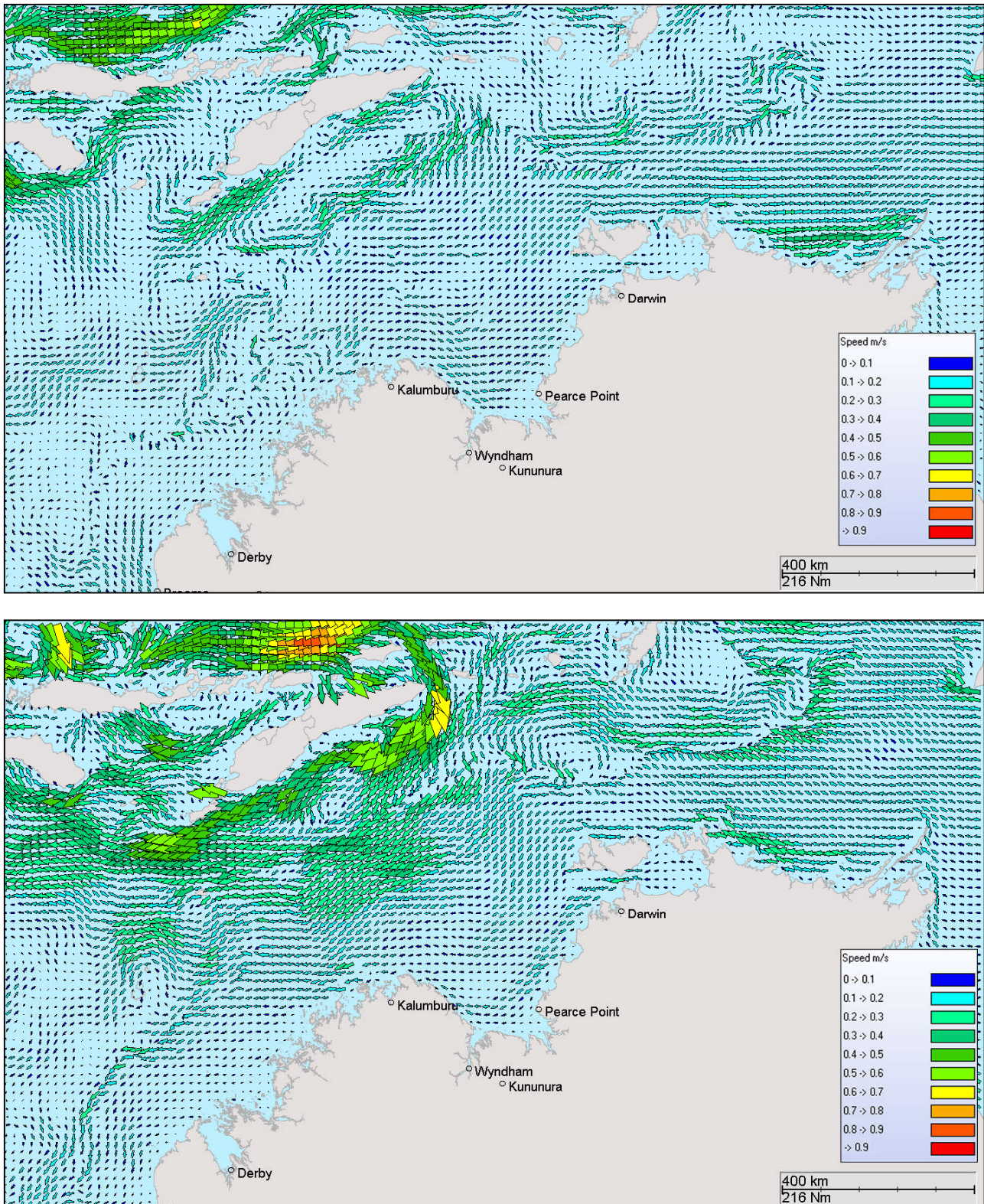
Figure 8 **Modelled HYCOM surface ocean currents on the 6th February 2012, summer conditions (upper image) and 11th May 2012, winter conditions (lower image). Derived from the HYCOM ocean hindcast model (Note: for image clarity only every 2nd vector is displayed).**

RPS Data Set Analysis

Current Speed (m/s) and Direction Rose (All Records)

Longitude = 130.19°E, Latitude = 9.88°S
Analysis Period: 01-Jan-2010 to 31-Dec-2010

Color Key [Current Speed(m/s)] :

| 0 - 0.01 | 0.01 - 0.1 | 0.1 - 0.2 | 0.2 - 0.3 | 0.3 - 0.4 | 0.4 - 0.5 | 0.5 - 0.6 | 0.6 - 0.7 | 0.7 - 0.8 | 0.8 - 0.9 | 0.9 - 1 |

*Calm defined as < 0.01
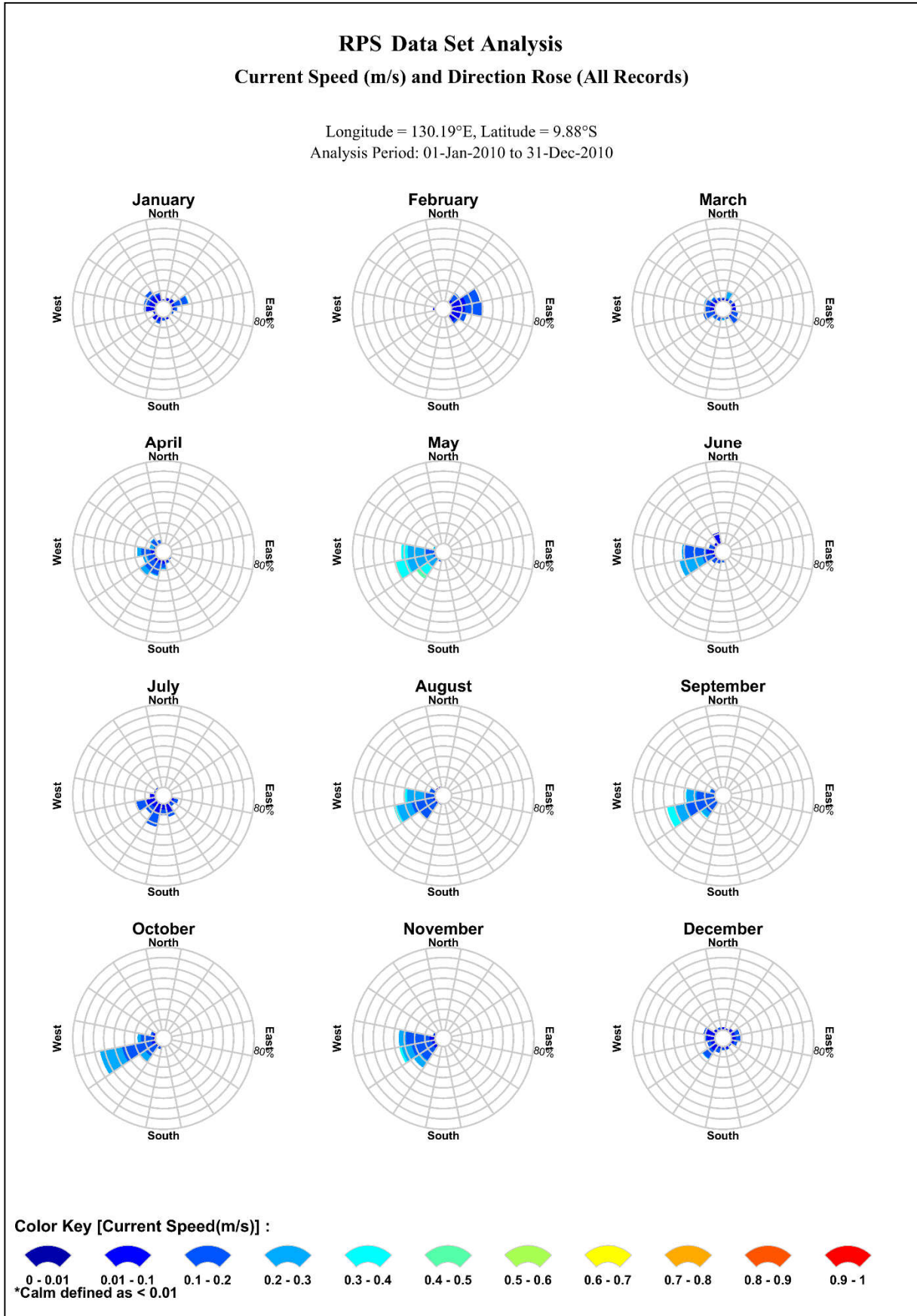
Figure 9 Monthly surface current rose plots adjacent to the model release location. Derived from analysis of HYCOM ocean data and tidal data for 2010 (La Niña year). The colour key shows the current speed (m/s), the compass shows the direction and the length of the wedge gives the percentage of the record for a particular speed and direction combination.

RPS Data Set Analysis

Current Speed (m/s) and Direction Rose (All Records)

Longitude = 130.19°E, Latitude = 9.88°S
Analysis Period: 01-Jan-2012 to 31-Dec-2012
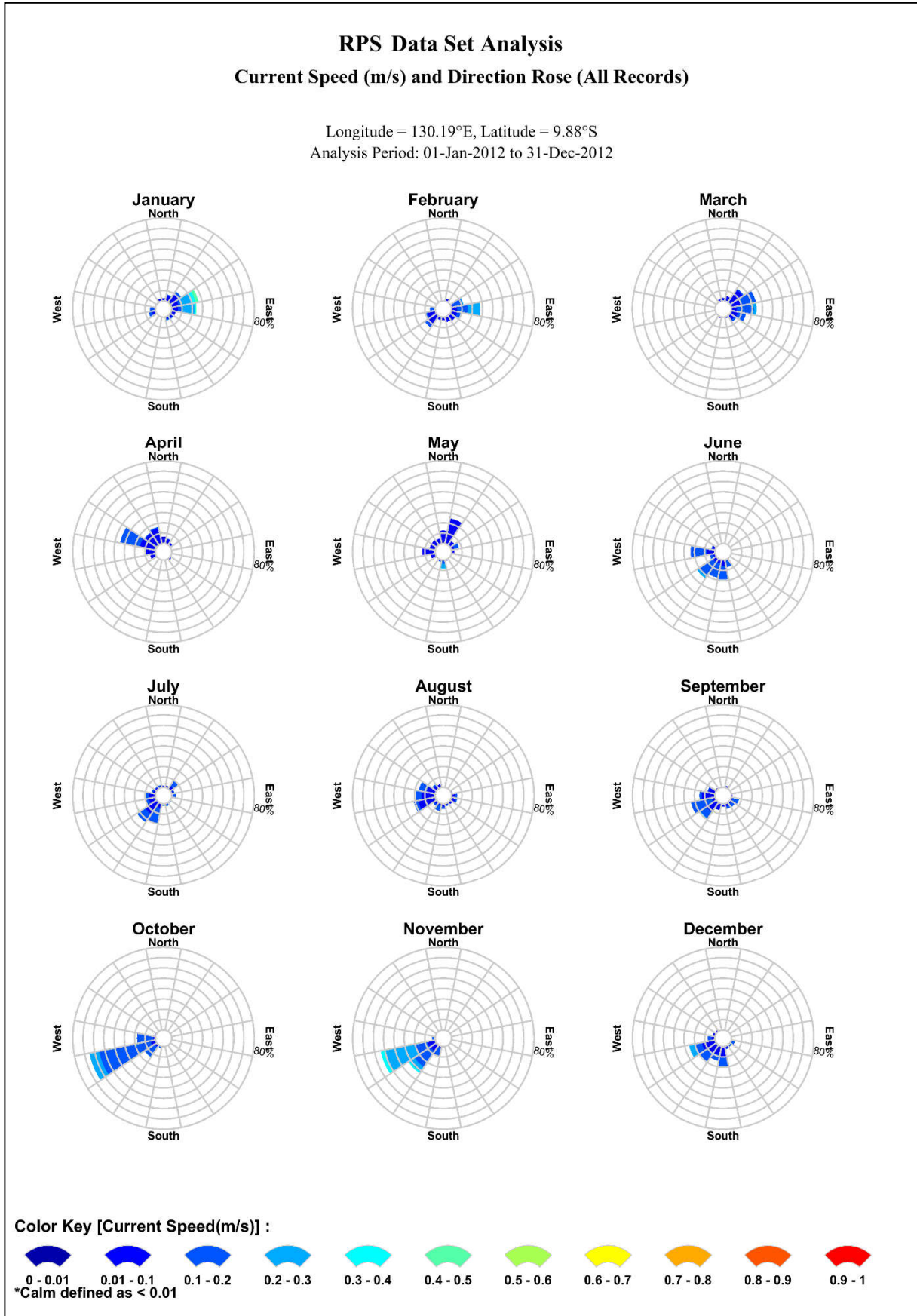
Figure 10 Monthly surface current rose plots adjacent to the model release location. Derived from analysis of HYCOM ocean data and tidal data for 2012 (neutral year). The colour key shows the current speed (m/s), the compass shows the direction and the length of the wedge gives the percentage of the record for a particular speed and direction combination.
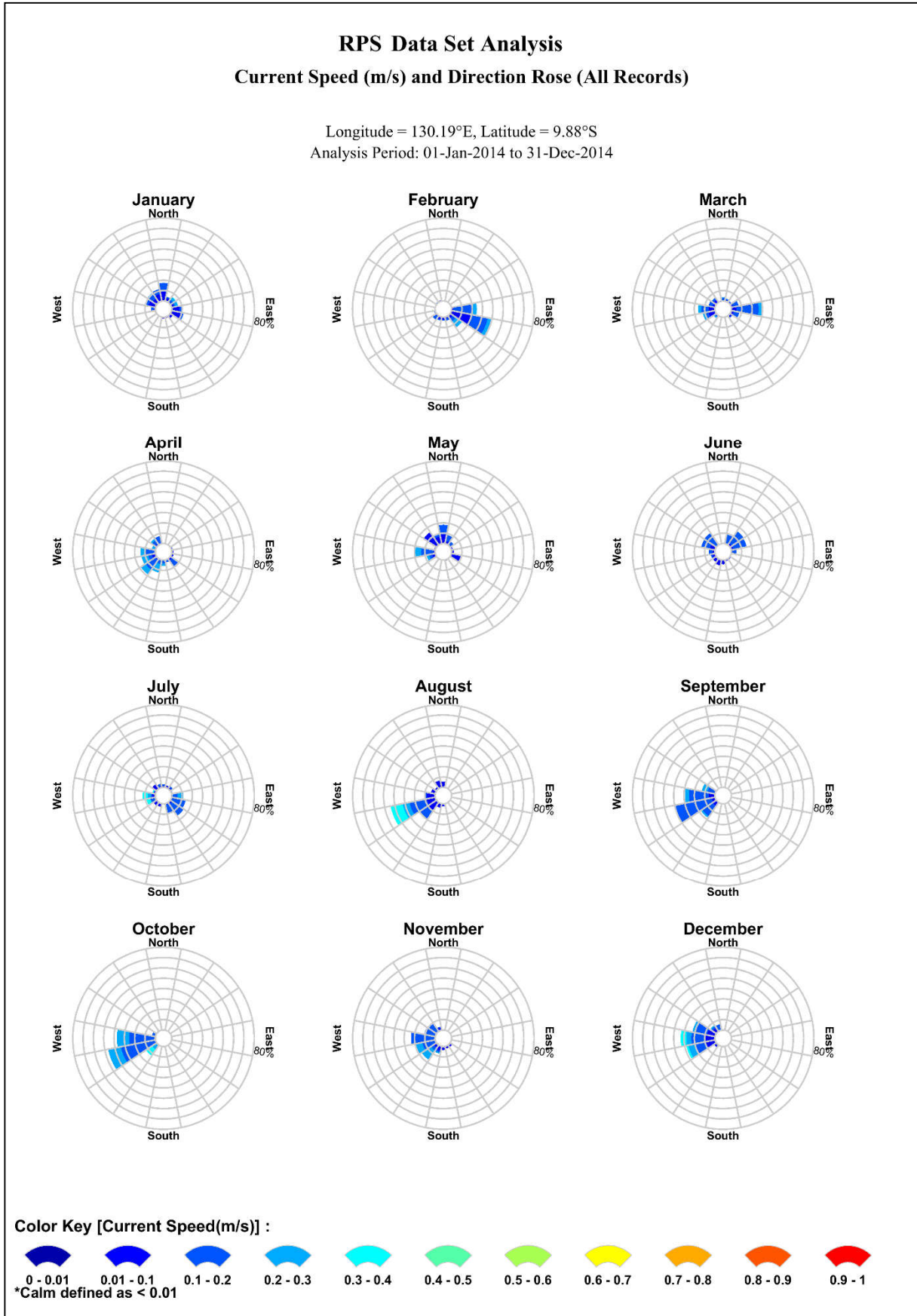
Figure 11 Monthly surface current rose plots adjacent to the model release location. Derived from analysis of HYCOM ocean data and tidal data for 2014 (El Niño year). The colour key shows the current speed (m/s), the compass shows the direction and the length of the wedge gives the percentage of the record for a particular speed and direction combination.

2.4.3   Tidal and current model validation

Fugro measured water levels and currents (speed and directions) at three locations within the Barossa offshore development area as part of the Barossa marine studies program (Figure 12, Fugro 2015). The measured data from the survey was made available to validate the predicted currents, which corresponds to the three identified seasons of the region (i.e. summer (December to February), transitional (March and September to November) and winter (April to August)).
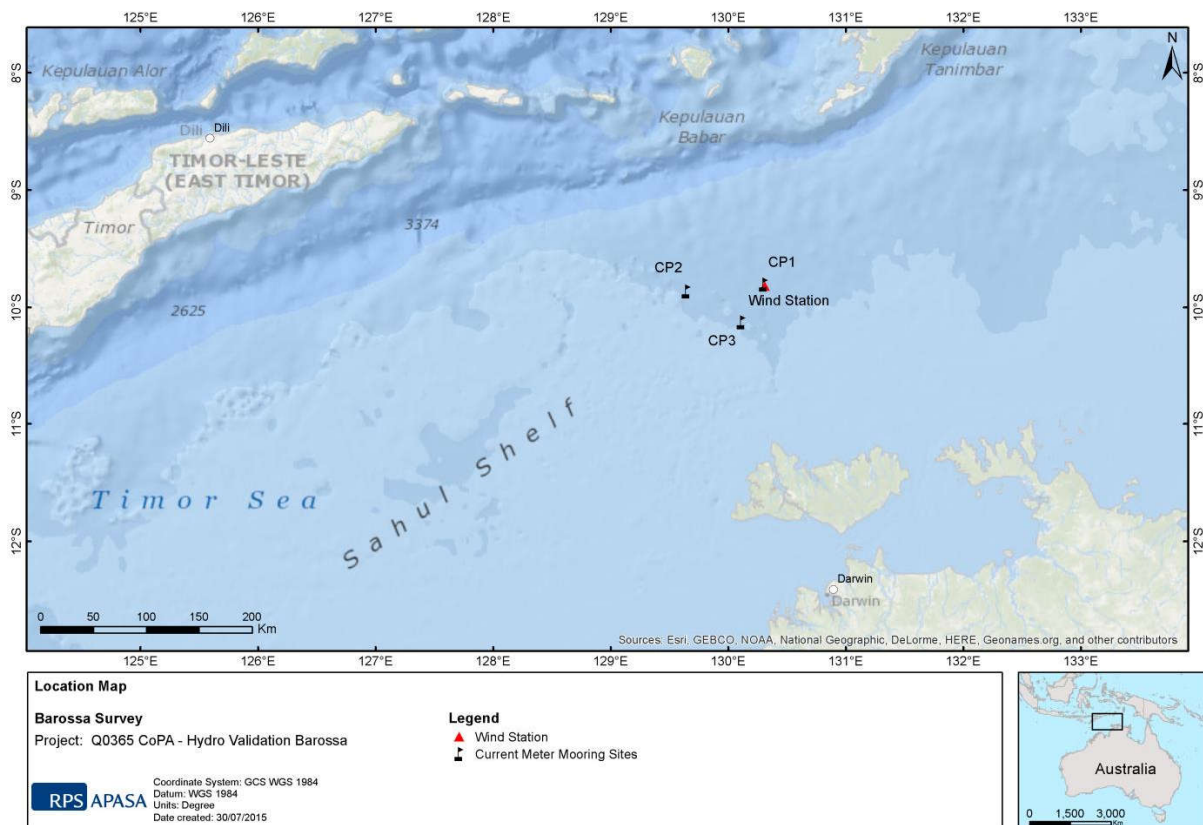
Figure 12 Locations of the CP1, CP2 and CP3 current meter moorings and the wind station

As an example, Figure 13 shows a comparison between the measured and predicted water levels at CP1 from 28 October 2014 to 14 March 2015. The figure shows a strong agreement in tidal amplitude and phasing throughout the entire deployment duration at the CP1 location.

To provide a statistical quantification of the model accuracy, comparisons were performed by determining the deviations between the predicted and measured data. As such, the root-mean square error (RMSE), root-mean square percentage (RMS %) and relative mean absolute error (RMAE) were calculated. Qualification of the RMAE ranges are reported in accordance with Walstra et al. (2001).

Table 6 shows the model performance when compared with measured water levels at CP1 from 28 October to 14 March 2015. According to the statistical measure, the HYDROMAP tidal model predictions were in very good agreement with the measured water levels at CP1.
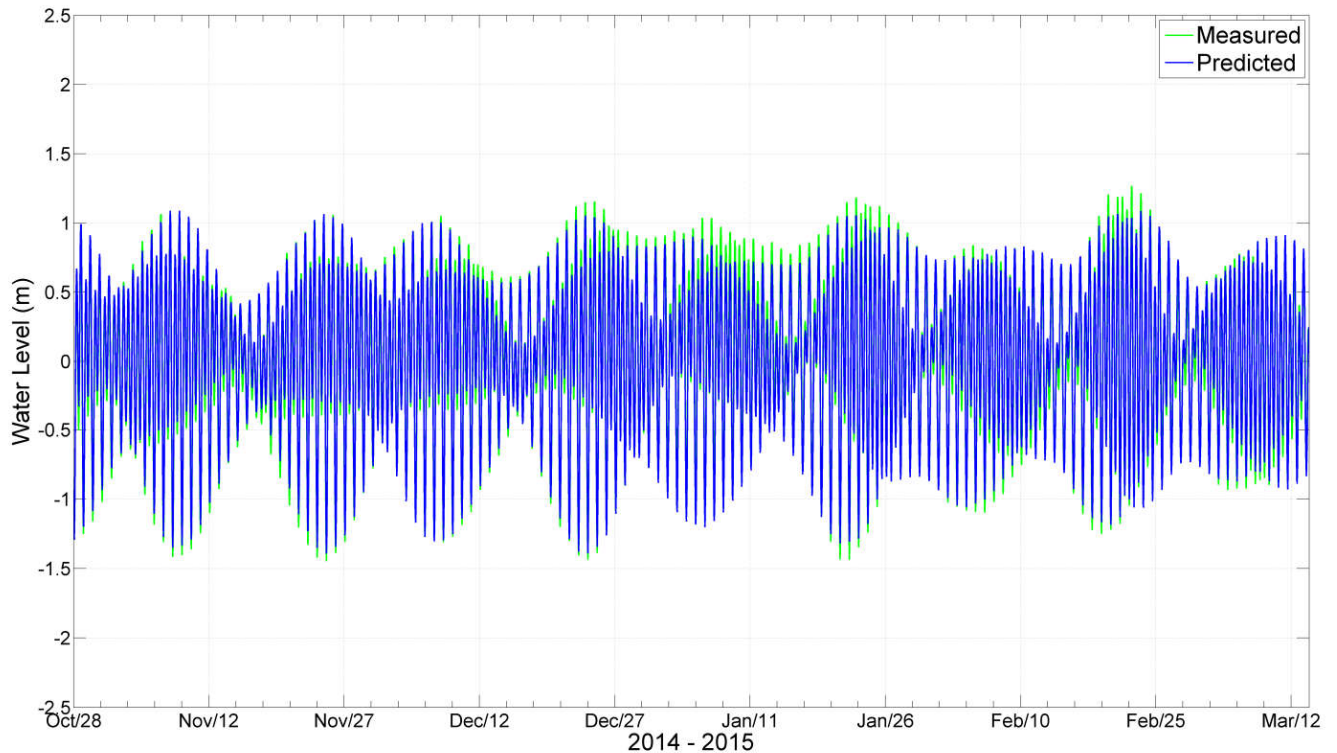
Figure 13 Comparison of measured and modelled water levels at CP1

Table 6 Statistical evaluation between measured water levels and HYDROMAP predicted water levels at CP1

Site	RMSE (m)	RMS (%)	RMAE	RMAE qualification
Mooring CP1	0.061	0.03	0.05	Very good

In addition, the HYCOM ocean currents combined with HYDROMAP tidal currents were compared to the measured current speed and directions from the CP1, CP2 and CP3 moorings. Figure 14 to Figure 16 show current comparison plots of the measured and predicted currents at each location for a range of depths (10 m, 50 m and 125 m BMSL) to highlight the differences between the wind-influenced surface layers and the mid water column.
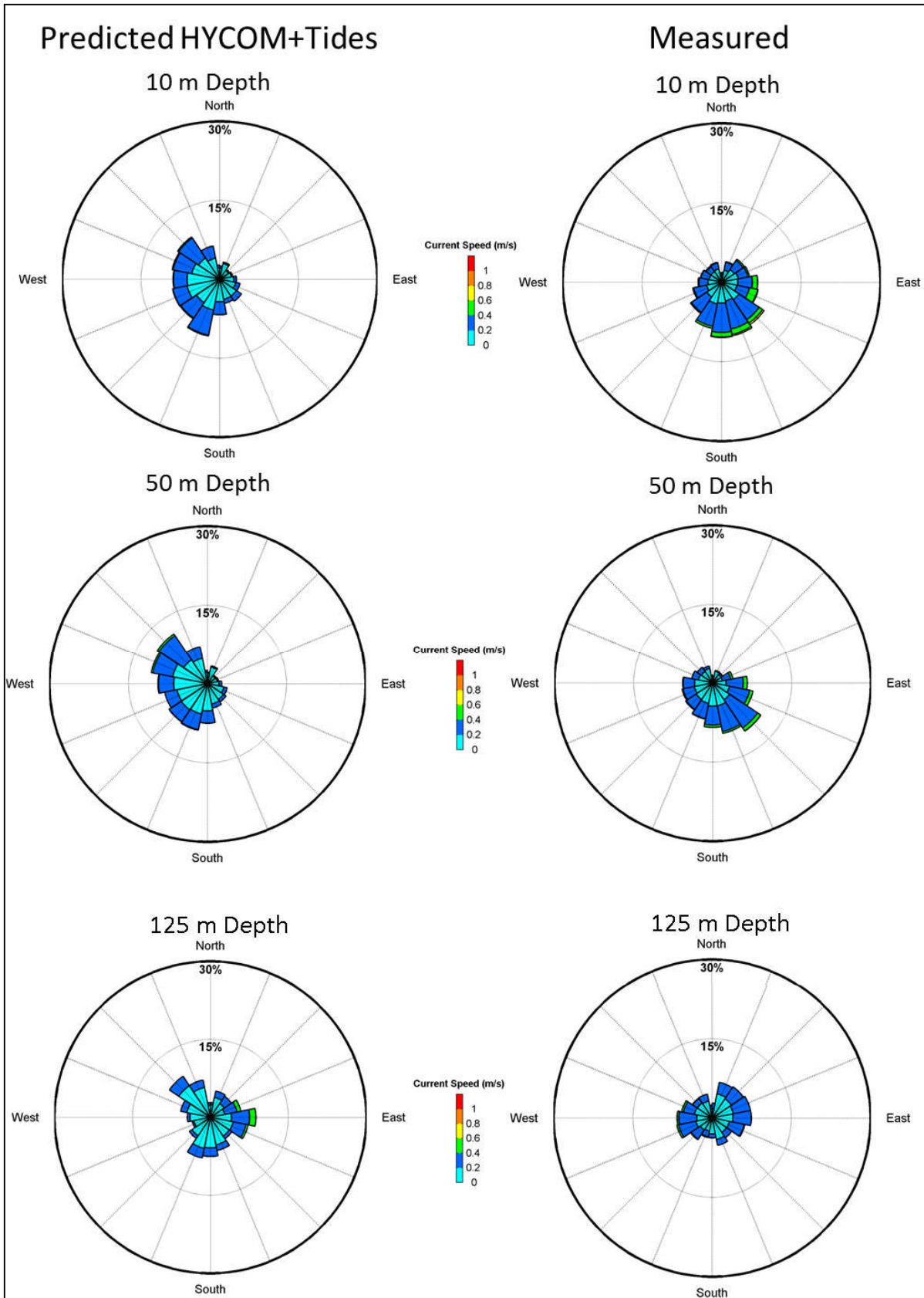
Figure 14 Comparison of predicted and measured current roses at CP1 from 9th July 2014 to 21st March 2015
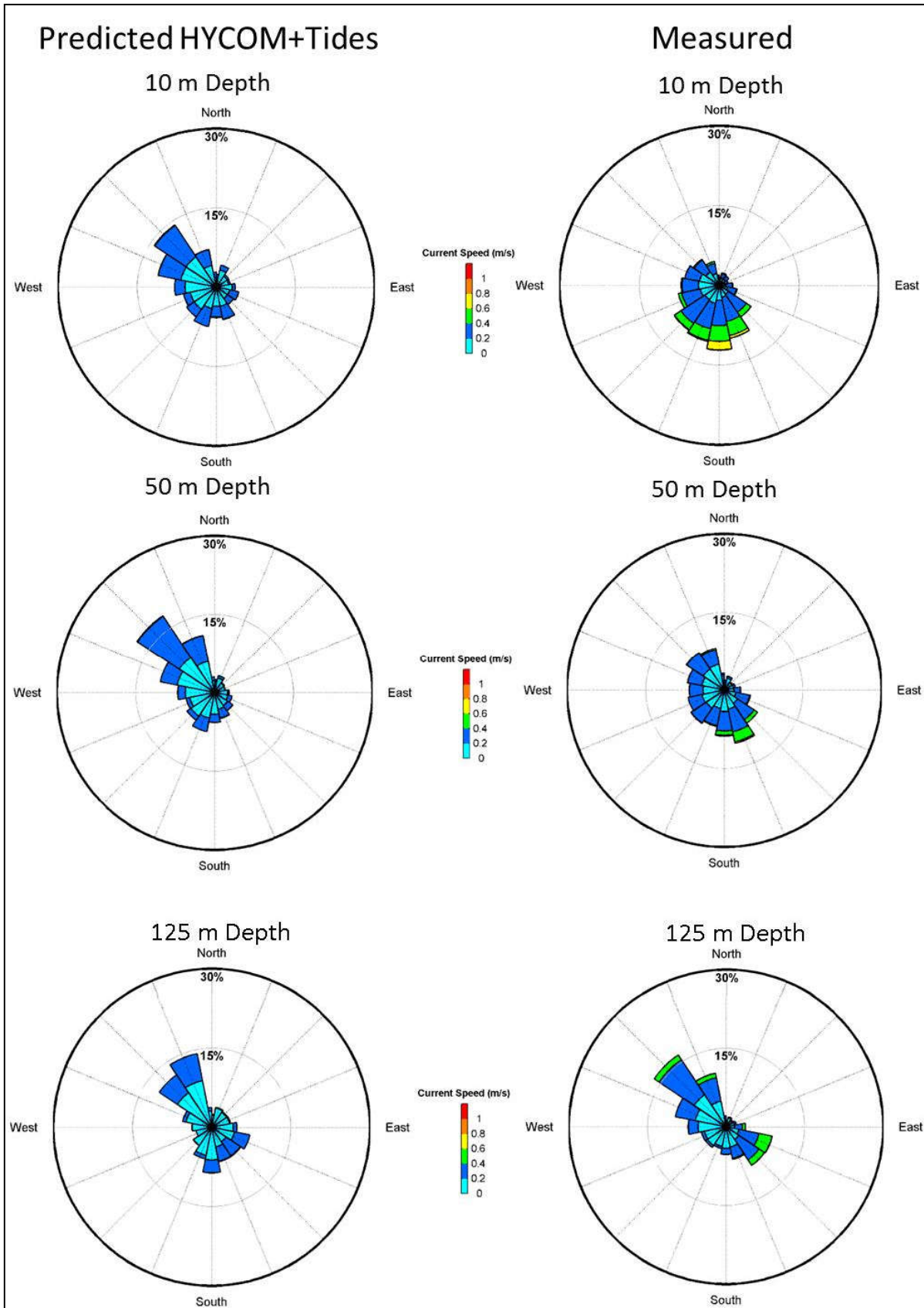
Figure 15 Comparison of predicted and measured current roses at CP2 from 10th July 2014 to 20st March 2015
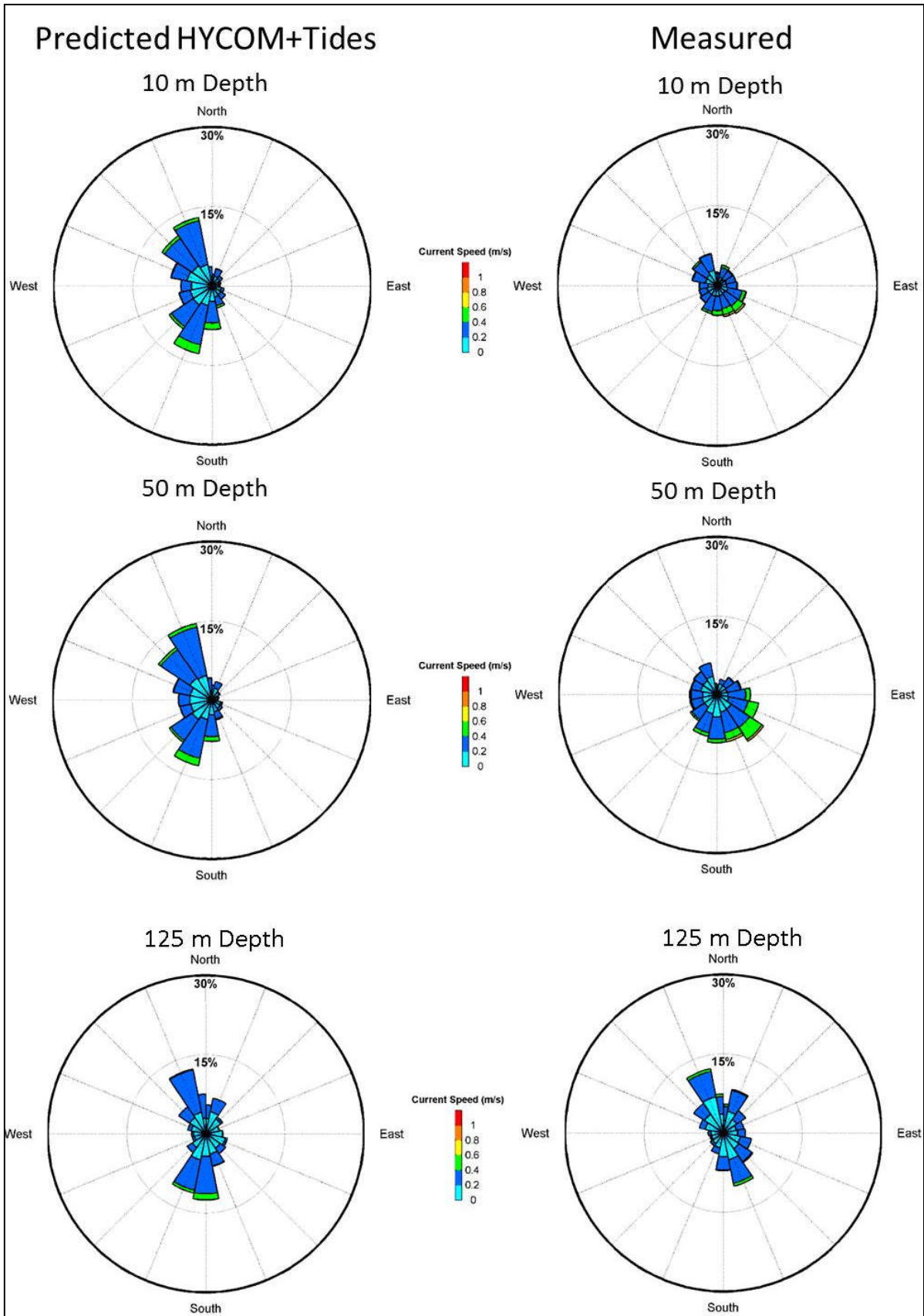
Figure 16 Comparison of predicted and measured current roses at CP3 from 9th July 2014 to 21st March 2015.

Overall, there was a good agreement between the predicted and measured currents at each site and depth. The model predictions were also able to recreate the two-layer flow which can be seen in the measured data and the reduction in current speeds as function of depth. From 10 m down to approximately 100 m below mean sea level (BMSL) the currents generally flowed south-east, with little variation due to tidal changes. The model predictions replicated this behaviour. Below 100 m, the influence of the tides became more pronounced, rotating between a south-eastward flow and a north-westward flow with the turning of the tide. Both tidal-scale and large-scale fluctuations in currents were typically reproduced at a similar magnitude and timing.

There was some divergence between the predicted and measured currents, mostly between data from July to October inclusive, due to the occurrence of solitons (or high frequency internal waves that can produce unusually high currents) which was highlighted by Fugro (2015). Despite these variations, the statistical comparisons between the measured and predicted current speeds indicate a reasonable to very good agreement (Table 7). Therefore, it can be concluded it is a good comparison and that the predicted current data reliably reproduced the complex conditions within the Barossa offshore development area and surrounding region. The RPS APASA (2015) model validation report provides a more detail regarding the tide and current comparison.

In summary, the Fugro (2015) data provides information specifically for the Barossa offshore development area and is considered the best available and most accurate data for this particular region. This data has been provided and reviewed by RPS to confirm predicted currents applied are accurate. As a result, the current data used herein is considered best available and highly representative of the characteristics influencing the marine environment in the Barossa offshore development area.

Table 7 Statistical evaluation between averaged measured currents and HYCOM ocean current and HYDROMAP tidal current at CP1, CP2 and CP3 at varying water depths (July 2014 to March 2015)

Site	Depth (m BMSL)	RMSE (m/s)	Measured peak value (m/s)	RMSE (%)	RMAE qualification
Mooring CP1	10	0.14	0.71	20	Good
	50	0.14	0.63	22	Very good
	125	0.13	0.61	22	Very good
Mooring CP2	10	0.16	0.82	19	Reasonable
	50	0.14	0.81	17	Good
	125	0.16	0.72	22	Reasonable
Mooring CP3	10	0.15	0.88	18	Very good
	50	0.14	0.78	18	Very good
	125	0.13	0.60	21	Very good

2.5   Environmental reporting criteria

The following environmental criteria were used for the modelling study.

Temperature

The criterion of assessing that temperature is within 3˚C within 100 m from the release location was applied for the PFW dispersion modelling study. This criterion represents a commonly adopted industry standard as part of the International Finance Corporation (IFC) Industry Environmental, Health and Safety Guideline for Offshore Oil and Gas Development (IFC 2015) for cooling water discharges, and is therefore not directly applicable to PFW. However, it has been used as a guide in the absence of any formally recognised criterion for PFW discharges.

Maximum extent of the plume

As the field is not yet producing, it is not possible to undertake ecotoxicological tests on the PFW. Therefore, the far-field modelling results are presented as dilution contour maps at intervals of 1:50, 1:75, 1:100, 1:150, 1:200, 1:300 and 1:500. Given an initial OIW concentration of 30 mg/L, the dilutions correspond to 0.6, 0.4, 0.3, 0.2, 0.15, 0.1 and 0.06 mg/L. This approach allows a direct comparison of the minimum dilutions for various chemicals (or whole stream) once ecotoxicological testing on actual Barossa operational discharges can be undertaken.

As a guide, the dissolved hydrocarbon thresholds from the Woodside Browse Floating LNG PFW were calculated to be 0.09 mg/L (or 0.09 ppm) based on Torosa condensate. This is equivalent to a dilution of 1:333 based on an initial OIW concentration 30 mg/L limit (Woodside Energy Ltd. 2011). It is understood that this threshold provides protection among the most sensitive of species (algae and copepods) and that the vast majority of species have higher tolerance compared to this threshold.

Based on RPS's experience and knowledge, ecotoxicological results from PFW discharges on the North West Shelf and in the Timor Sea shows that a dilution of 1:300 (or 0.1 mg/L concentration) is a conservative threshold for species protection for no effect concentration.

Additionally, the far-field modelling was used to calculate the distance to achieve an OIW concentration of ≤ 7 µg/L, representing a 99% species protection level based on ANZECC/ARMCANZ (2000) guidelines. This is equivalent to a dilution of 1:4,285 based on an initial OIW concentration of 30 mg/L limit.

3.0 Modelling results

3.1 Near-field modelling

Figure 17 to Figure 22 (note the differing x- and y-axis aspect ratios) show the change in minimum temperature and dilution of the PFW plume under the varying flow rates (minimum and maximum), seasonal conditions (summer, transitional and winter) and current speeds (weak, medium and strong). The figures show the predicted distances travelled by the plume along the horizontal before contacting the sea surface.

The results showed that due to the momentum of the PFW discharge, a turbulent mixing zone was created approximately 1 m below the discharge pipe which is 10 m below the water surface. The increased flow rate only marginally changed (<0.2 m) the depth of the predicted mixing zone. While the increased ambient current strengths were shown to slightly reduce the plunge depth, the stronger currents did considerably force the plume further horizontally from the discharge pipe.

Following the initial plunge, the plume remained buoyant enough to rise to the surface for both flow rates (1,590 m^3/d and 3,260 m^3/d) and all current strengths. As the plume rose through the water column, it continued to mix with ambient waters, however as the plume approached the sea surface the rate of mixing slowed.

Table 8 to Table 9 show the predicted plume characteristics varying flow rates, seasonal conditions and current speeds. The strong currents were capable of pushing the buoyant plume horizontally up to a maximum distance of 36.3 m during the 1,590 m^3/d flow rate and 26.3 m during the 3,260 m^3/d flow rate, allowing for additional mixing prior to reaching the surface. The plume for the lower discharge rate had travelled further before reaching the water surface. The diameter of the PFW plume at the sea surface ranged from 3.0 m to 10.6 m during weak and strong currents under 1,590 m^3/d flow rate and 2.9 m to 10.0 m during weak and strong currents under 3,260 m^3/d flow rate conditions.

In all cases, the temperature of the PFW plume was predicted to be within 3°C of the ambient (background) temperature within 100 m from the release location. Appendix A and Appendix B provide graphs of the predicted difference in temperature between the PFW plume and ambient temperature versus distance from release location for the 1,590 m^3/d and 3,260 m^3/d flow rates, respectively. The temperature of the PFW plume generally returned to within 3°C of ambient water temperature within 2 m horizontally from the release location.

For all seasons and flow rates modelled, the primary factor influencing dilution of the PFW, was the strength of the ambient current. Weak currents had little effect on the plume during the rise process and therefore, it reached the sea surface quickly, slowing the rate of dilution (see Table 8 to Table 9 and Figure 17 to Figure 22). The average dilutions of the PFW plume upon encountering the sea surface under medium and strong constant currents were predicted to be >1:190 during the 1,590 m^3/d flow rate and >1:89 during 3,260 m^3/d flow rate, respectively. Additionally, the minimum dilutions of the PFW plume (i.e. dilution of plume centreline) upon encountering the sea surface under medium and strong constant currents were predicted to be >1:66 during the 1,590 m^3/d flow rate and >1:37 during 3,260 m^3/d flow rate, respectively. Note that these predictions rely on the persistence of current speed and direction over time and does not account for the build-up of the plume.

Figure 17 Near-field average temperature and dilution results for constant weak, medium and strong summer currents (1,590 m³/d flow rate).

Figure 18 Near-field average temperature and dilution results for constant weak, medium and strong transitional currents (1,590 m³/d flow rate).

Figure 19 Near-field average temperature and dilution results for constant weak, medium and strong winter currents (1,590 m³/d flow rate).

Figure 20 Near-field average temperature and dilution results for constant weak, medium and strong summer currents (3,260 m³/d flow rate).
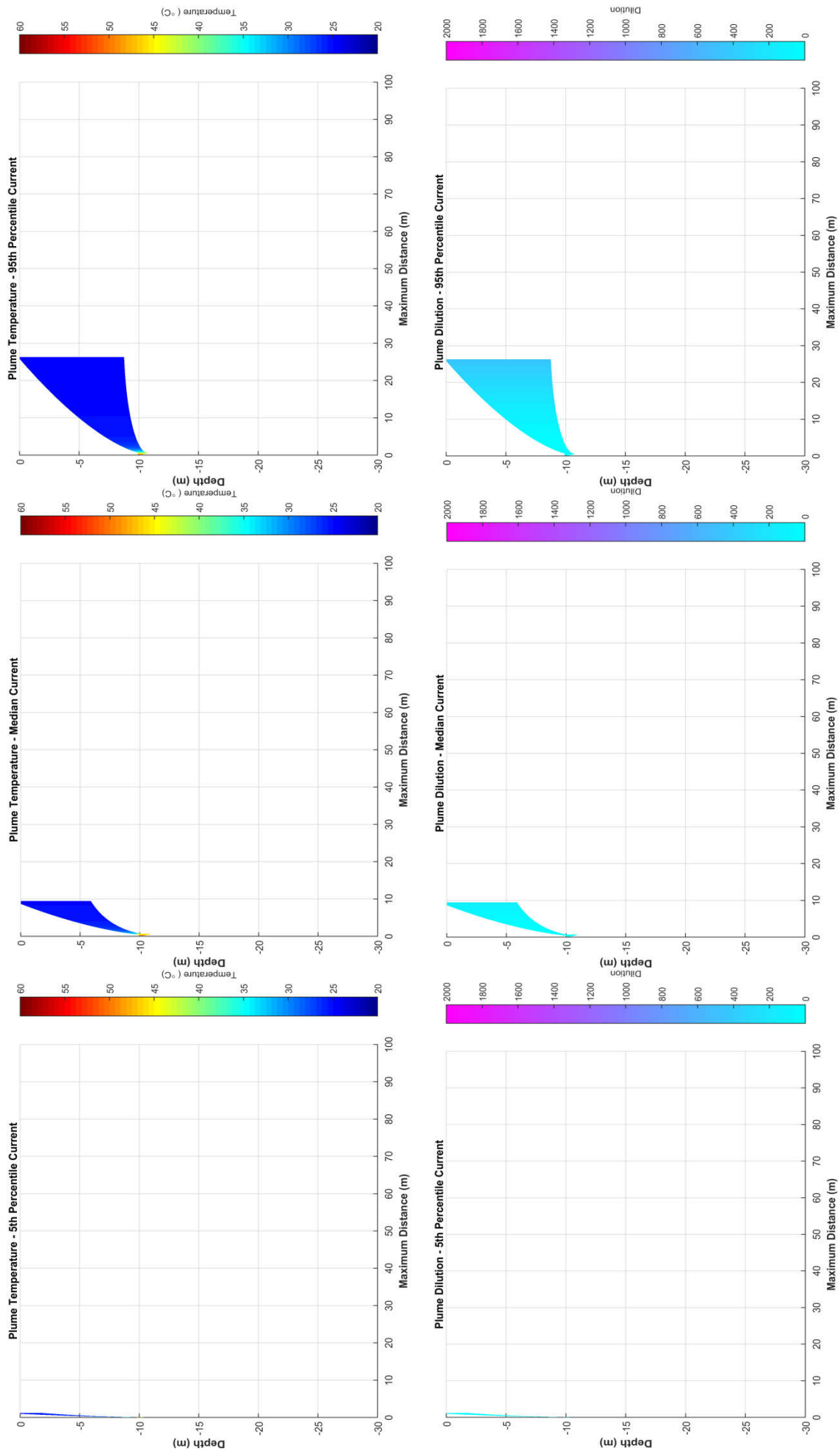
Figure 21 Near-field average temperature and dilution results for constant weak, medium and strong transitional currents (3,260 m³/d flow rate).
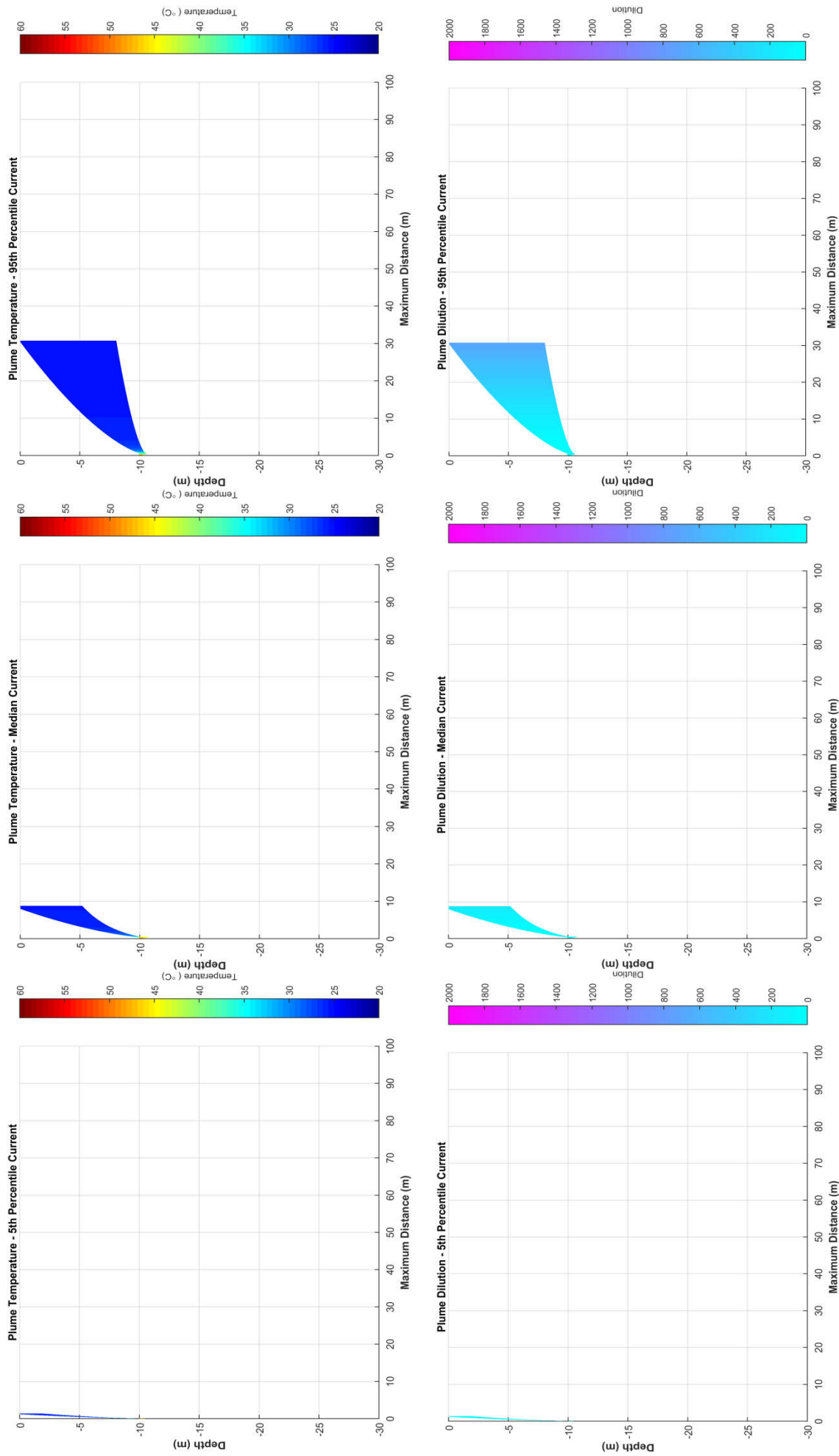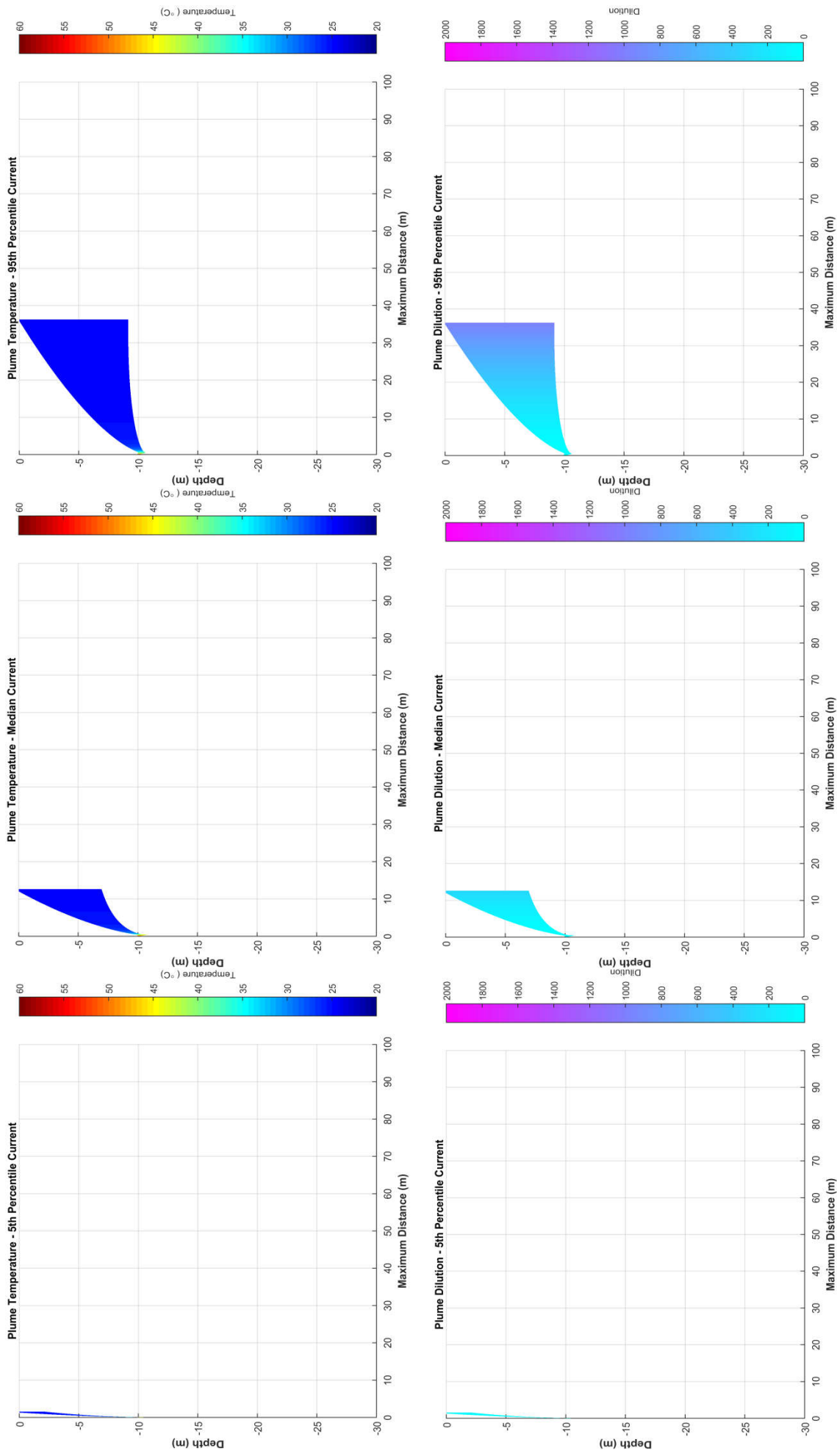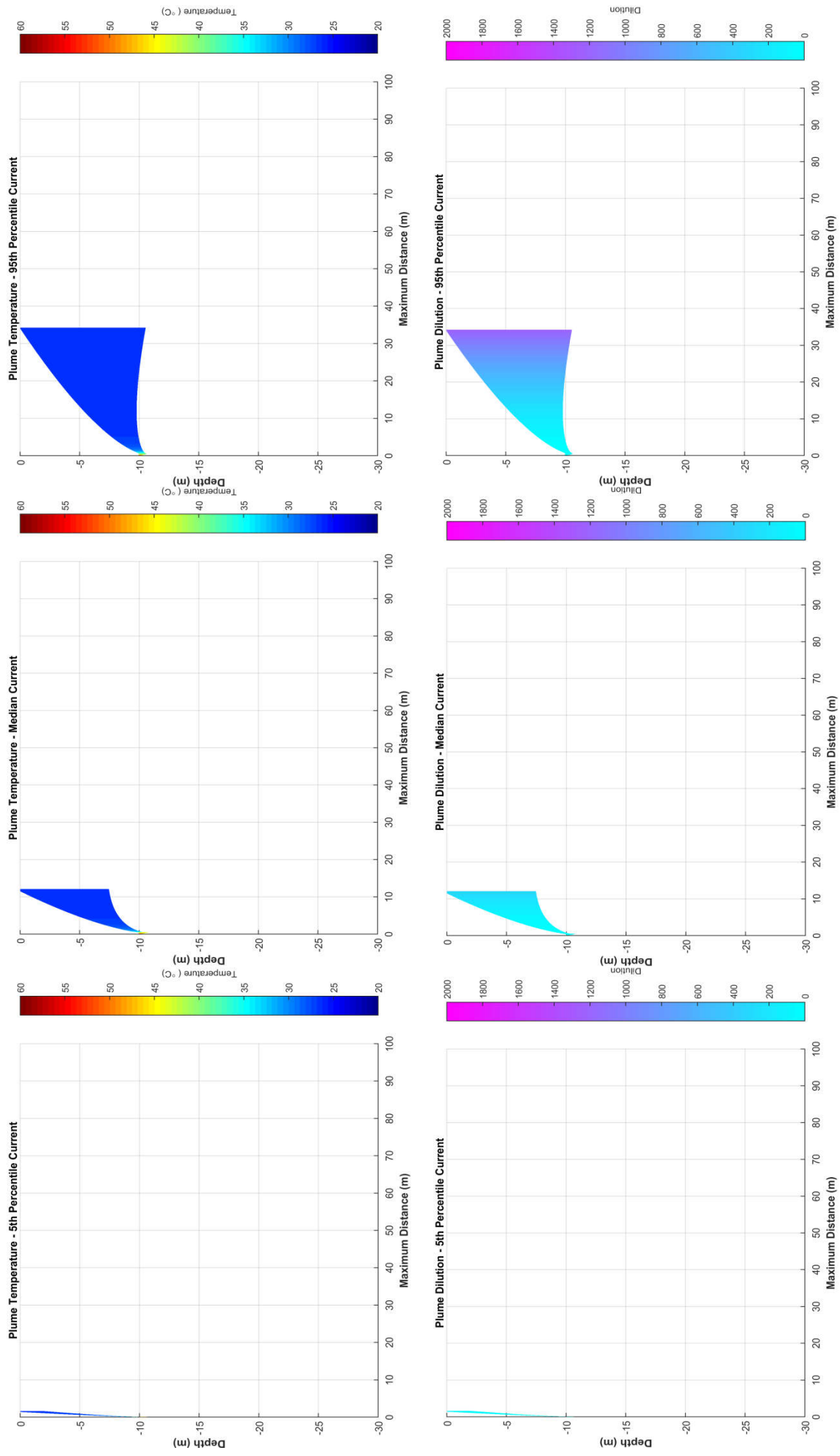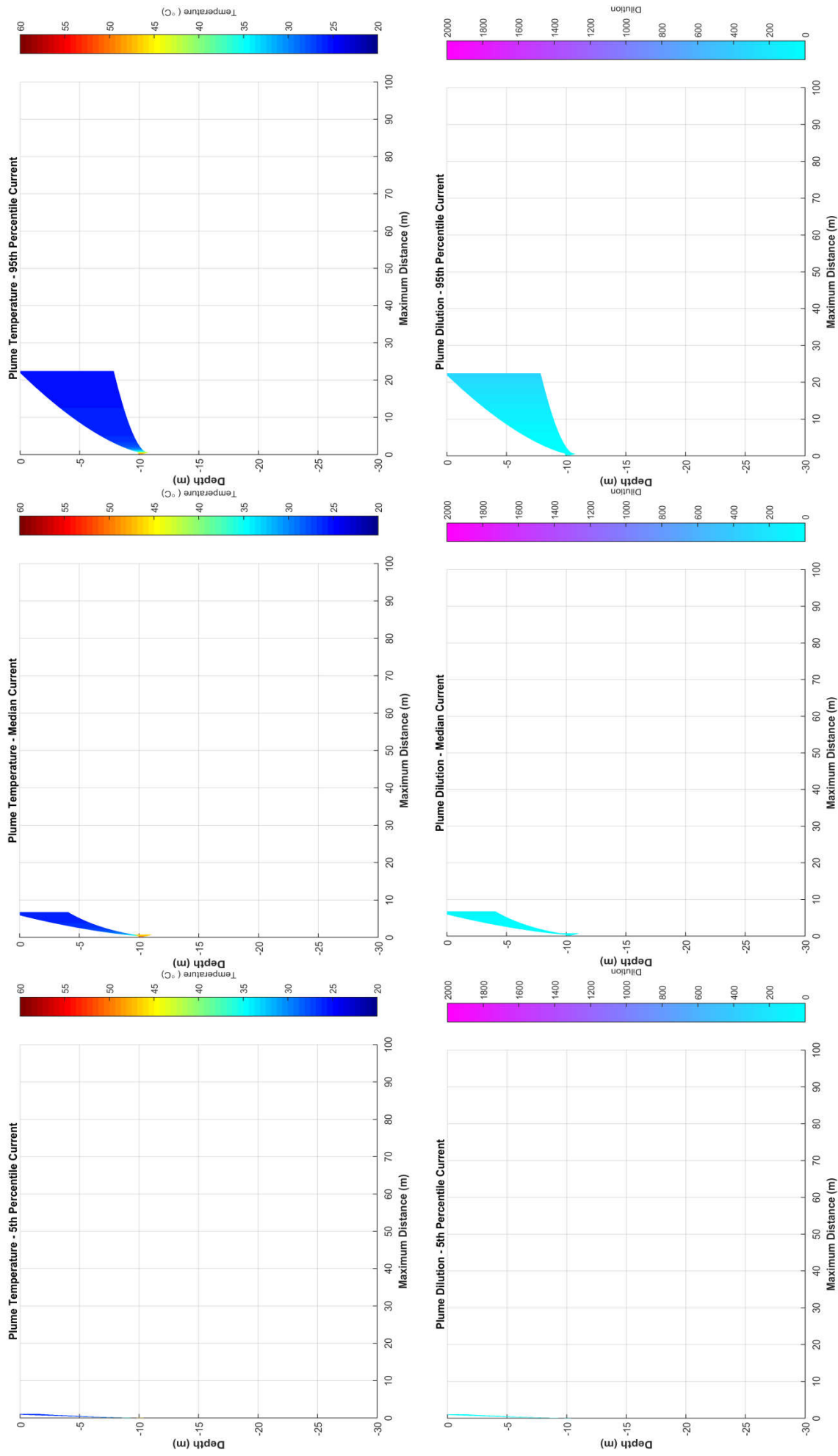
RPS
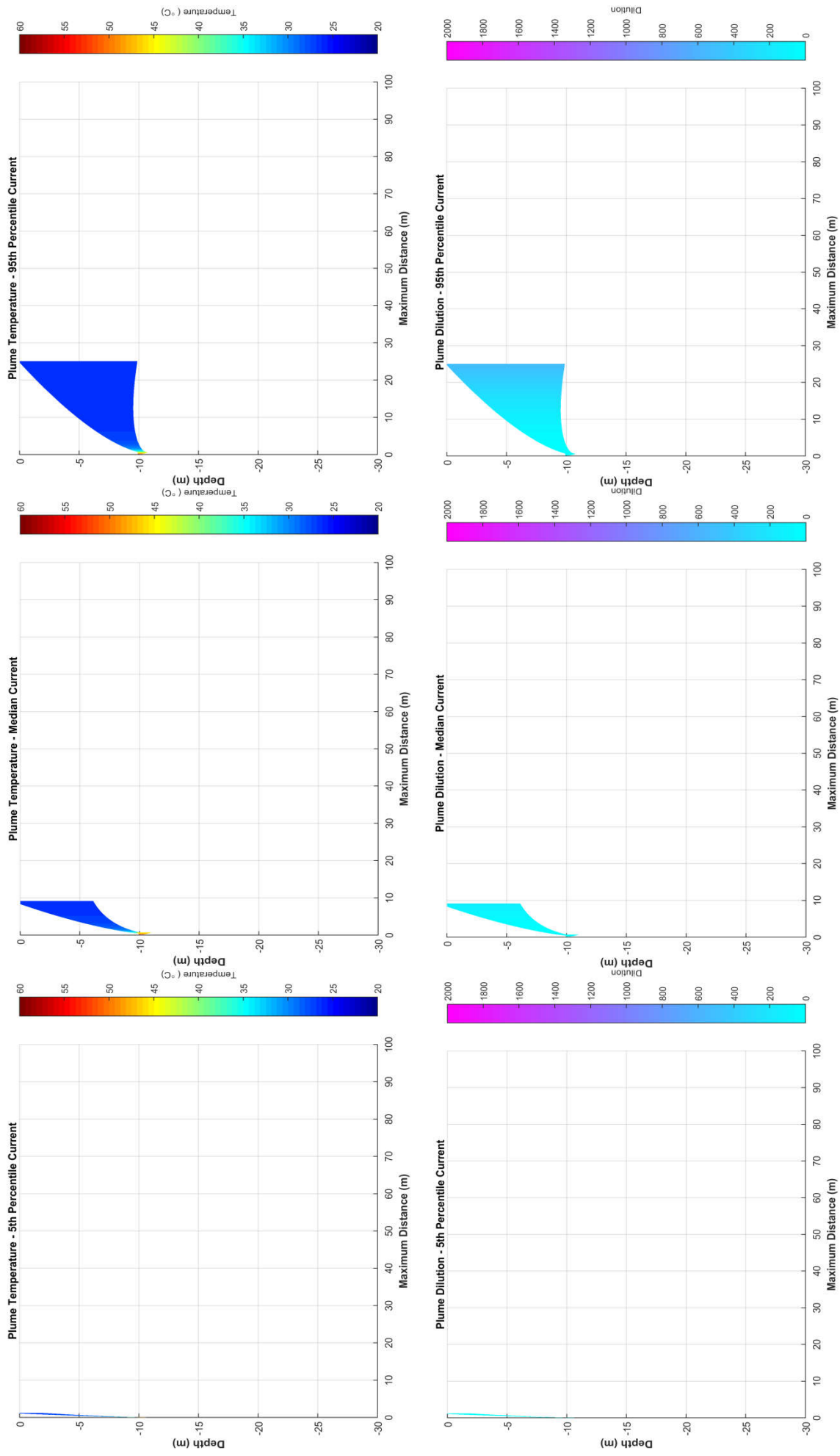
Figure 22 Near-field average temperature and dilution results for constant weak, medium and strong winter currents (3,260 m³/d flow rate).

Table 8 Predicted plume characteristics upon encountering the sea surface (end of near-field mixing) for the minimum flow rate (1,590 m³/d flow) for each season and current speed.

Season	Surface current speed (m/s)	Plume diameter at the sea surface (m)	Plume temperature (°C)	Difference between plume and ambient temperature (°C)	Dilution of the plume (1:x)		Maximum horizontal distance (m)
					Minimum	Average	
Summer	Weak (0.04)	3.0	25.9	0.5	34	67	1.4
	Medium (0.11)	5.9	25.6	0.2	66	190	8.8
	Strong (0.27)	8.1	25.5	0.1	177	698	30.8
Transitional	Weak (0.05)	3.4	25.2	0.5	38	76	1.6
	Medium (0.14)	7.3	24.8	0.1	92	318	12.7
	Strong (0.29)	9.2	24.7	0.0	253	992	36.3
Winter	Weak (0.03)	3.3	26.7	0.4	39	76	1.6
	Medium (0.11)	7.8	26.4	0.1	102	329	12.1
	Strong (0.27)	10.6	26.3	0.0	314	1,224	26.3

Table 9 Predicted plume characteristics upon encountering the sea surface (end of near-field mixing) for the maximum flow rate (3,260 m³/d flow) for each season and current speed.

Season	Surface current speed (m/s)	Plume diameter at the sea surface (m)	Plume temperature (°C)	Difference between plume and ambient temperature (°C)	Dilution of the plume (1:x)		Maximum horizontal distance (m)
					Minimum	Average	
Summer	Weak (0.04)	2.9	26.3	0.9	20	40	1.1
	Medium (0.11)	5.1	25.8	0.4	37	89	6.8
	Strong (0.27)	8.0	25.5	0.1	87	336	22.5
Transitional	Weak (0.05)	3.1	25.5	0.8	22	44	1.2
	Medium (0.14)	6.5	25.0	0.3	47	140	9.5
	Strong (0.29)	8.9	24.8	0.1	116	451	26.3
Winter	Weak (0.03)	3.2	27.0	0.7	23	45	1.2
	Medium (0.11)	6.9	26.5	0.2	51	141	9.2
	Strong (0.27)	10.0	26.4	0.1	139	534	25.1

3.2   Far-field modelling

3.2.1   General observations

Figure 23 to Figure 24 show screenshots of predicted dilutions (equivalent concentrations) for the OIW every 2 hours from 12 pm to 10 pm on the 10th December 2010. The results are based on the maximum flow rate of 3,260 m³/d.

The images have been included to illustrate that the concentrations (and in turn dilutions) became more variable over time as a result of the change in current directions and speeds. Higher dilutions (lower concentrations) were predicted during periods of increased current speeds, whereas patches of lower dilutions (higher concentrations) tended to accumulate during the turn of the tide and/or during prolonged periods of decreased current speeds. During these periods of decreased current speed, the plume had a more continuous appearance, with the higher concentration patches moving as a unified group. These findings are in agreement with the research of King and McAllister (1997, 1998) who also noted that concentrations of oil within PFW plumes generated by the Harriet Alpha platform (located on the North West Shelf of Western Australia) were patchy and peak around the turn of the tides. Furthermore, the far-field modelling results demonstrated that due to the buoyant nature of the plume, the plume predominantly remained in the 0 m–10 m surface waters.

Figure 25 shows time series graphs of the OIW dilutions at 4 compass points (north, east, west and south) 100 m from the release location during December 2010 conditions (3,260 m³/d flow rate). As the graph shows, high dilutions of 1:3,000 were achieved daily within 100 m of the release location, over the 31 day period in all four directions.
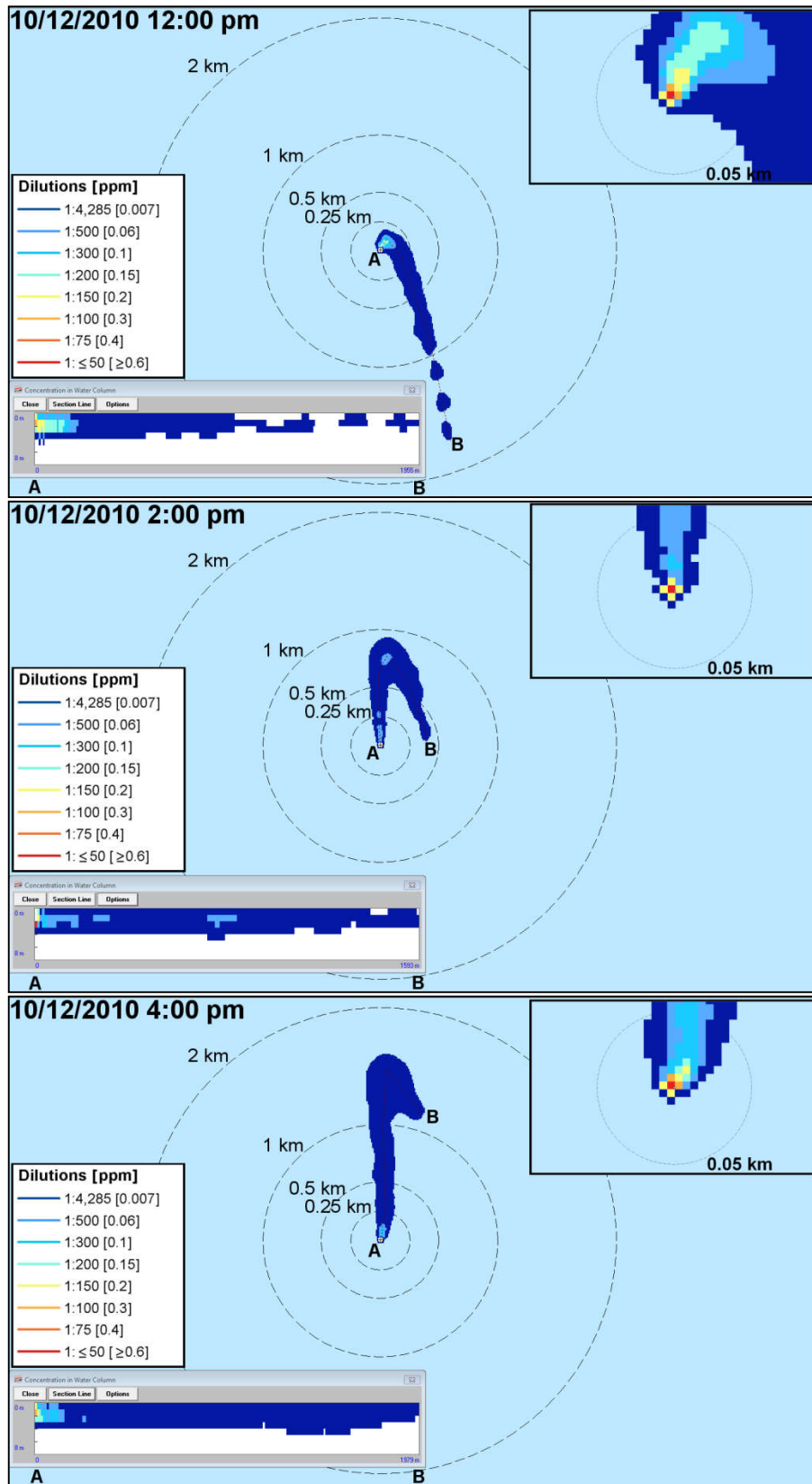
Figure 23 Screenshots every 2 hours of the predicted OIW dilutions (and equivalent concentration, mg/L) from 12 pm to 4 pm 10th December 2010. Results are based on the surface waters (0-1 m depth) for the maximum discharge rate scenario (3,260 m³/d flow with 30 mg/L initial OIW concentration). Figure insets illustrate zoomed-in view of predicted plume dilutions.
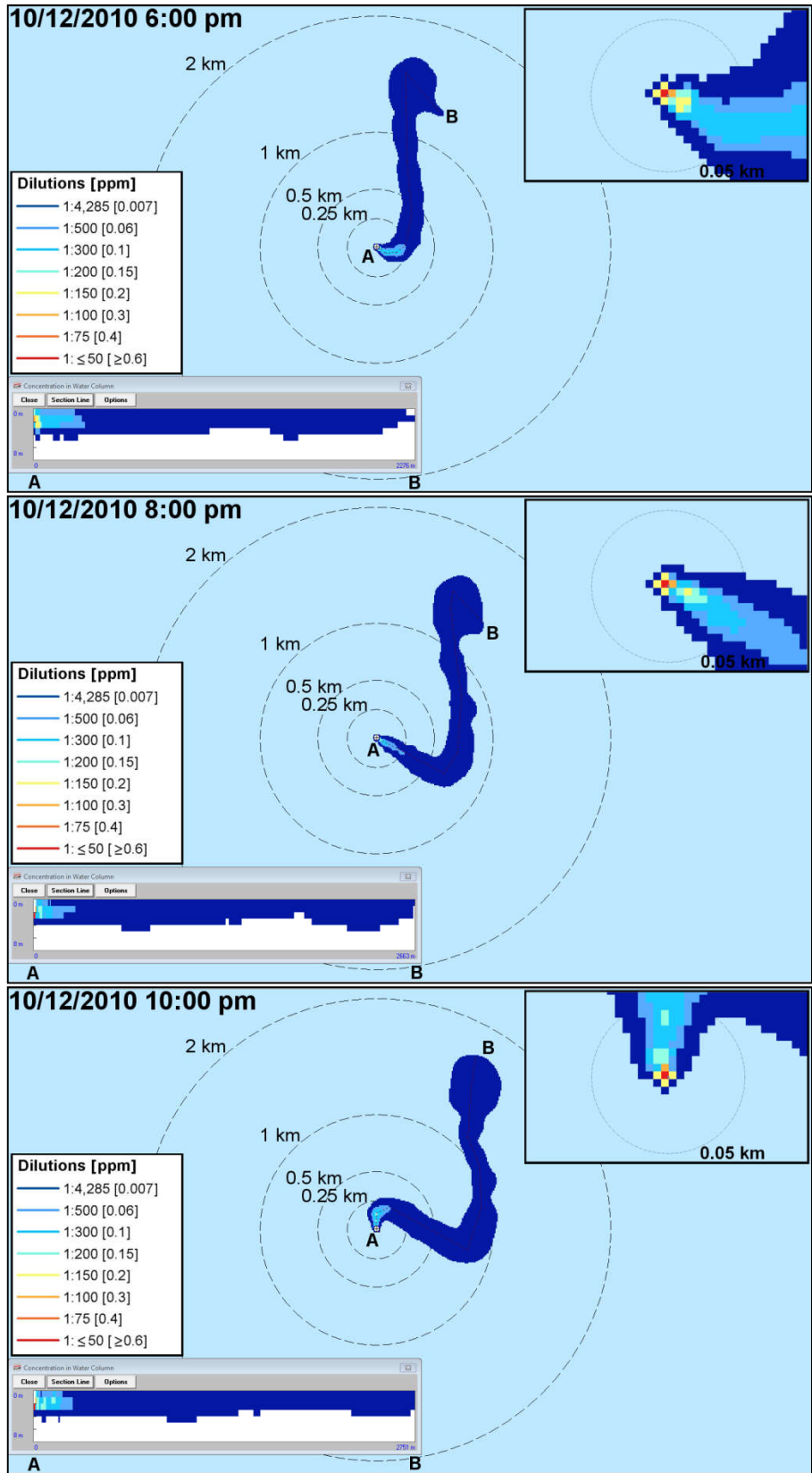
Figure 24 Screenshots every 2 hours of the predicted OIW dilutions (and equivalent concentration, mg/L) from 6 pm to 10 pm 10th December 2010. Results are based on the surface waters (0-1 m depth) for the maximum discharge rate scenario (3,260 m³/d flow with 30 mg/L initial OIW concentration). Figure insets illustrate zoomed-in view of predicted plume dilutions.
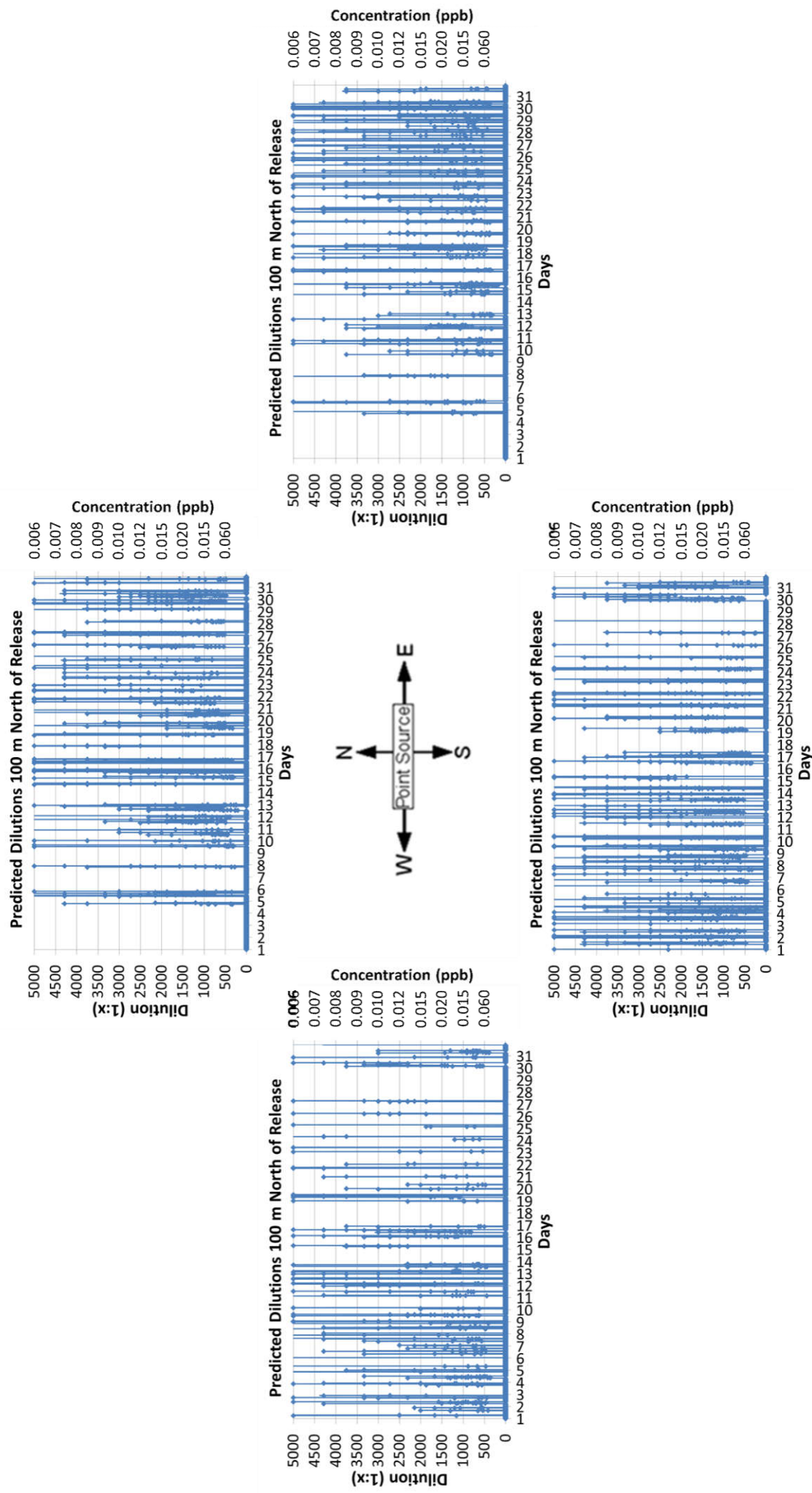
Figure 25 Predicted OIW dilutions at four compass points (north, east, west and south), 100 m from the release location during December 2010 conditions and maximum flow rate (3,260 m³/d)

3.2.2   Seasonal analysis

The 10 minute model outputs for each month from each of the three years (2010, 2012 and 2014) were combined and analysed according to the respective season (i.e. summer – December, January, February; transitional periods – March, April and September to November; and winter – May to August). This approach assists with identifying the potential for exposure on a seasonal basis, to the nearest shoals/banks to the Barossa offshore development area (i.e. Evans Shoal, Tassie Shoal and Lynedoch Bank) whilst taking into account the interannual variability.

Table 10 shows the minimum dilution achieved at specific distances from the release location for each flow rate and season.

Table 11 provides a summary of the maximum distances from the release location to achieve a given dilution for each flow rate and season. Dilutions of 1:4,285 (equivalent to approximately 7 µg/L, which represents a 99% species protection level based on ANZECC/ARMCANZ (2000) guidelines) were predicted to occur between 3.45 km to 4.57 km from the release location for the 1,590 m^3/d flow rate and 5.53 km to 6.07 km for the 3,260 m^3/d flow rate. Based on the maximum distance from the 1:4,285 dilution contour to the nearest shoal/bank being Evans Shoal (minimum distance of approximately 59.4 km and 57.9 km, respectively) no exposure is expected to non-transient species. However, pelagic species may come into contact with the plume and may be exposed intermittently.

Table 12 presents the total area of coverage for a given dilution for each flow rate and season. Based on the 1,590 m^3/d flow rate and 1:4,285 dilution, the area of exposure was largest during the summer conditions (6.31 km^2) and smallest during the transitional months (4.29 km^2). The extent was found to be influenced by the rate of discharge. For example, by increasing the flow rate to 3,260 m^3/d and maintaining the initial OIW concentration of 30 mg/L, the 1:4,285 dilution area increased by approximately 96% for the summer conditions (from 6.31 km^2 to 12.39 km^2).

Figure 26 to Figure 31 show the extent of the minimum dilutions (under 2010, 2012 and 2014 conditions) for each flow rate and season assuming an initial OIW concentration of 30 mg/L. Note that the images represent the lowest predicted dilution (highest concentration) at any given time-step through the water column and do not take into account frequency or duration.

Table 10 Minimum dilution achieved at specific distances from the PFW discharge release location for each flow rate and season.

Flow rate (m^3/d)	Season	Minimum achieved dilution at specific distances from the release location						
		0.1 km radius	0.5 km radius	1 km radius	2 km radius	3 km radius	5 km radius	> 5 km radius
1,590	Summer	1:300	1:500	1:4,285	1:4,285	1:4,285	>1:4,285	>1:4,285
	Transitional	1:200	1:4,285	1:4,285	1:4,285	1:4,285	>1:4,285	>1:4,285
	Winter	1:200	1:500	1:500	1:4,285	1:4,285	>1:4,285	>1:4,285
3,260	Summer	1:100	1:300	1:500	1:500	1:4,285	1:4,285	1:4,285
	Transitional	1:100	1:200	1:500	1:4,285	1:4,285	1:4,285	1:4,285
	Winter	1:100	1:300	1:500	1:500	1:4,285	1:4,285	1:4,285

Table 11 Maximum distance from the PFW discharge release location to achieve a given dilution for each flow rate and season.

Flow rate (m³/d)	Season	Maximum distance (km) from release location to achieve given dilution							
		1:50 dilution	1:75 dilution	1:100 dilution	1:150 dilution	1:200 dilution	1:300 dilution	1:500 dilution	1:4,285 dilution
1,590	Summer	<0.01	0.01	0.02	0.02	0.07	0.16	0.48	3.45
	Transitional	<0.01	0.01	0.02	0.02	0.06	0.15	0.41	3.88
	Winter	<0.01	0.01	0.02	0.02	0.07	0.18	0.49	4.57
3,260	Summer	0.02	0.04	0.07	0.11	0.30	0.68	2.26	5.91
	Transitional	0.02	0.03	0.06	0.10	0.29	0.71	1.90	5.53
	Winter	0.02	0.04	0.07	0.11	0.35	0.76	2.88	6.07

Table 12 Total area of coverage for a given dilution for each flow rate and season.

Flow rate (m3/d)	Season	Total area (km²) of coverage for a given dilution							
		1:50 dilution	1:75 dilution	1:100 dilution	1:150 dilution	1:200 dilution	1:300 dilution	1:500 dilution	1:4,285 dilution
1,590	Summer	<0.001	<0.001	<0.001	<0.001	0.005	0.024	0.15	6.31
	Transitional	<0.001	<0.001	<0.001	<0.001	0.003	0.018	0.11	4.29
	Winter	<0.001	<0.001	<0.001	<0.001	0.005	0.024	0.16	6.18
3,260	Summer	<0.001	<0.001	0.003	0.004	0.049	0.178	1.10	12.40
	Transitional	<0.001	<0.001	0.003	0.003	0.041	0.158	0.91	8.93
	Winter	<0.001	<0.001	0.004	0.004	0.049	0.178	1.11	11.97

Figure 26 Predicted OIW dilutions under summer conditions for the minimum PFW flow rate (1,590 m³/d).

Figure 27 Predicted OIW dilutions under transitional conditions for the minimum PFW flow rate (1,590 m³/d)

Figure 28 Predicted OIW dilutions under winter conditions for the minimum PFW flow rate (1,590 m³/d).
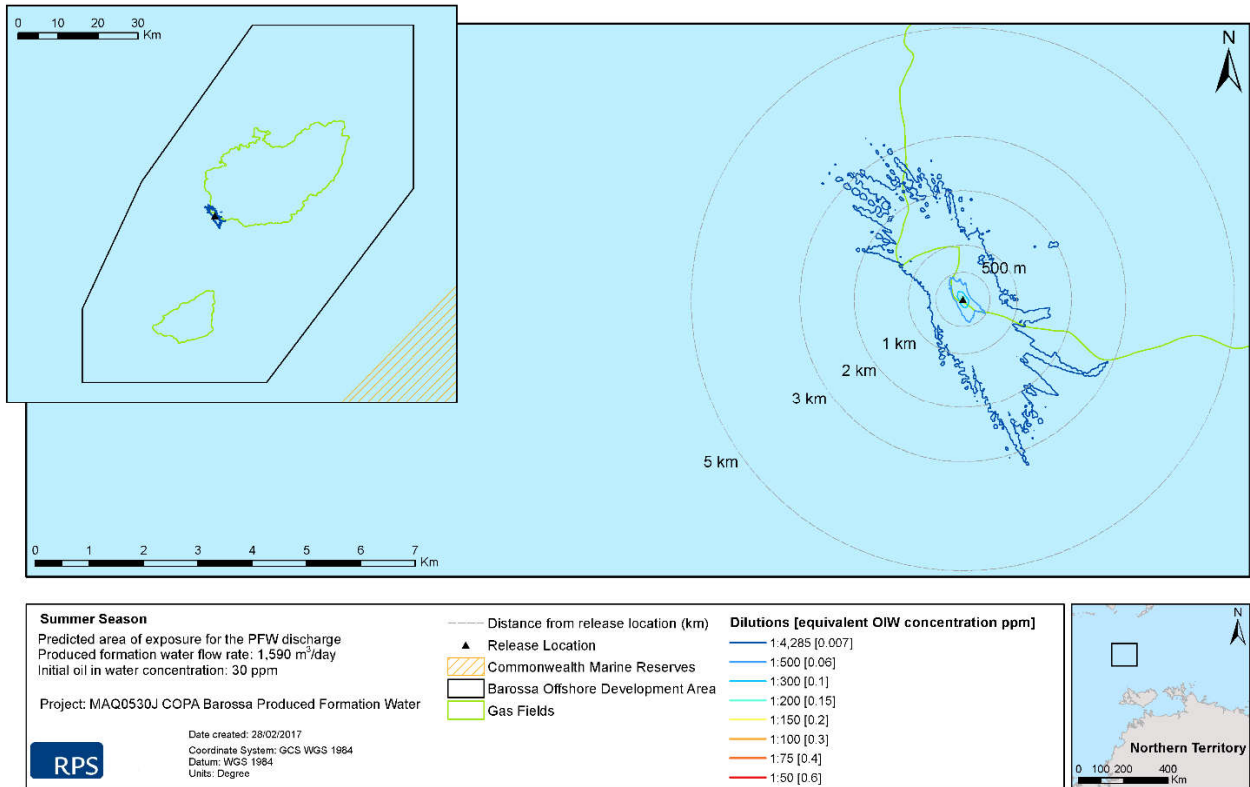

Figure 29 Predicted OIW dilutions under summer conditions for the maximum PFW flow rate (3,260 m³/d).
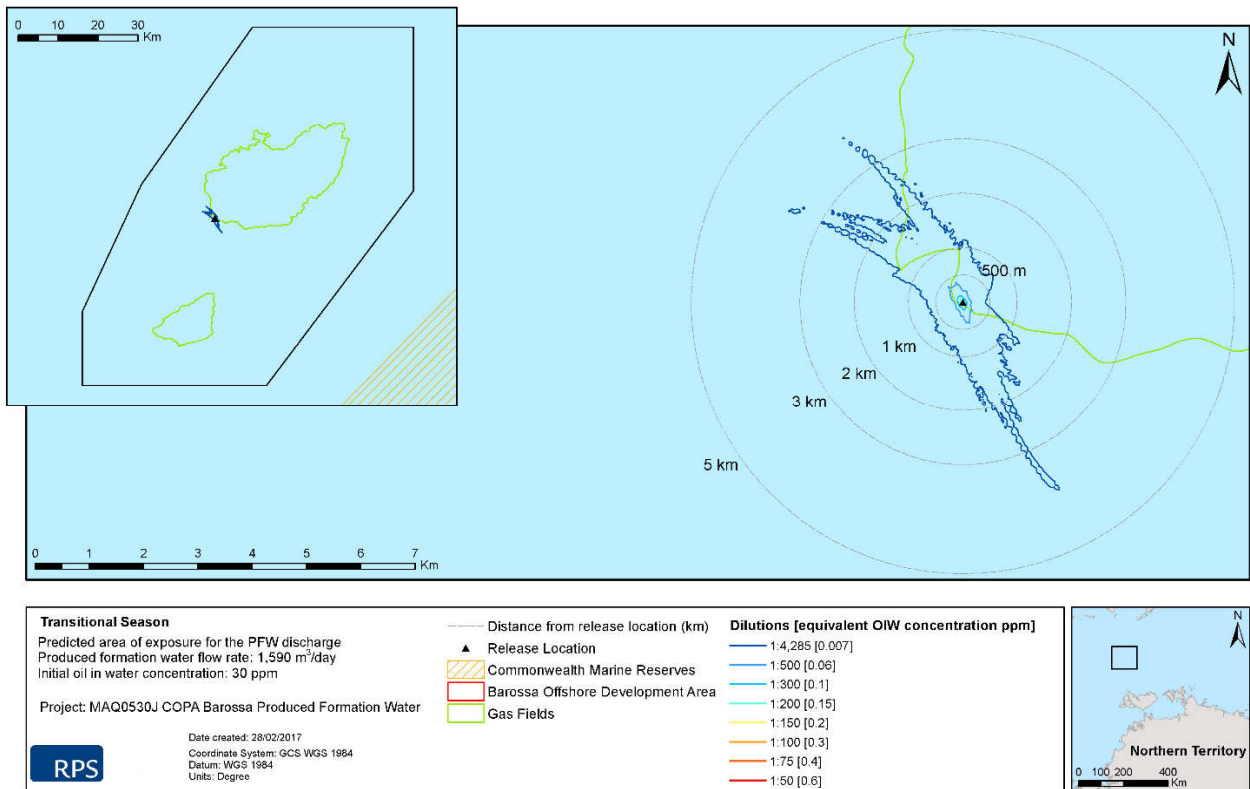
Figure 30 Predicted OIW dilutions under transitional conditions for the maximum PFW flow rate (3,260 m³/d).
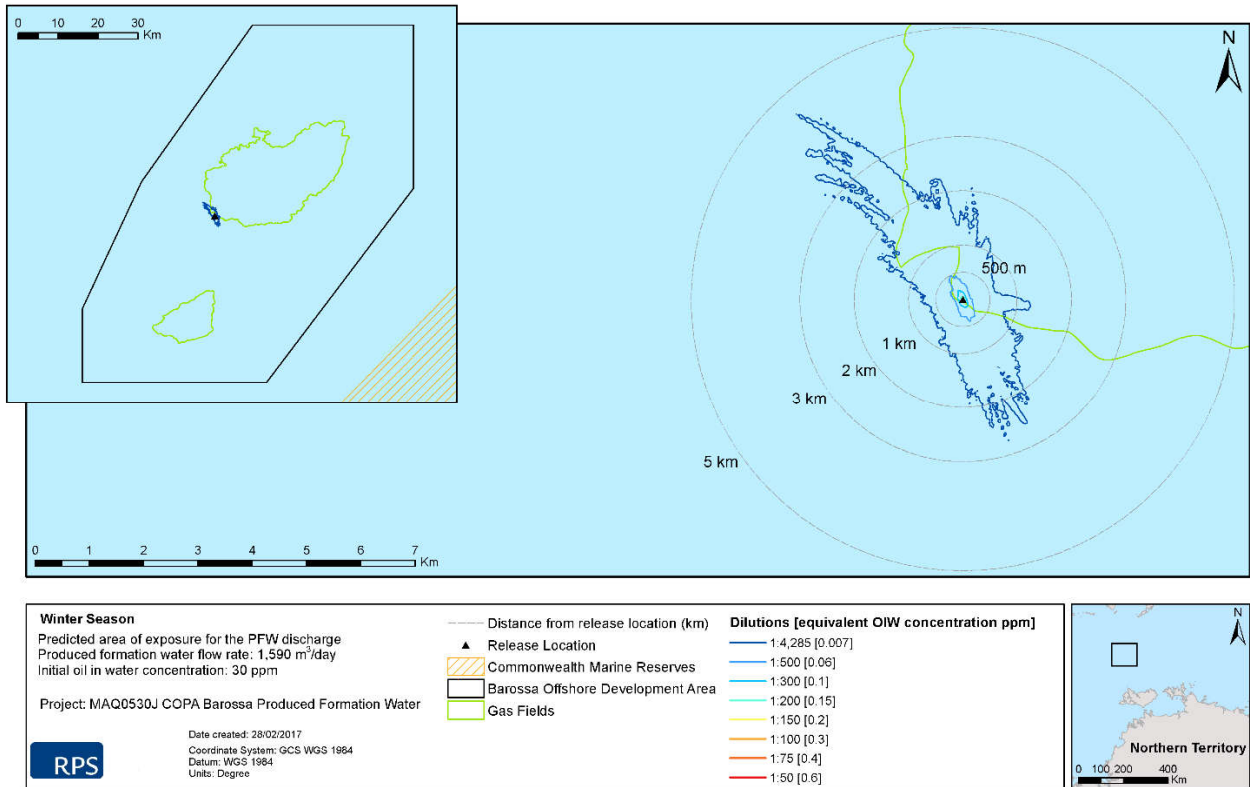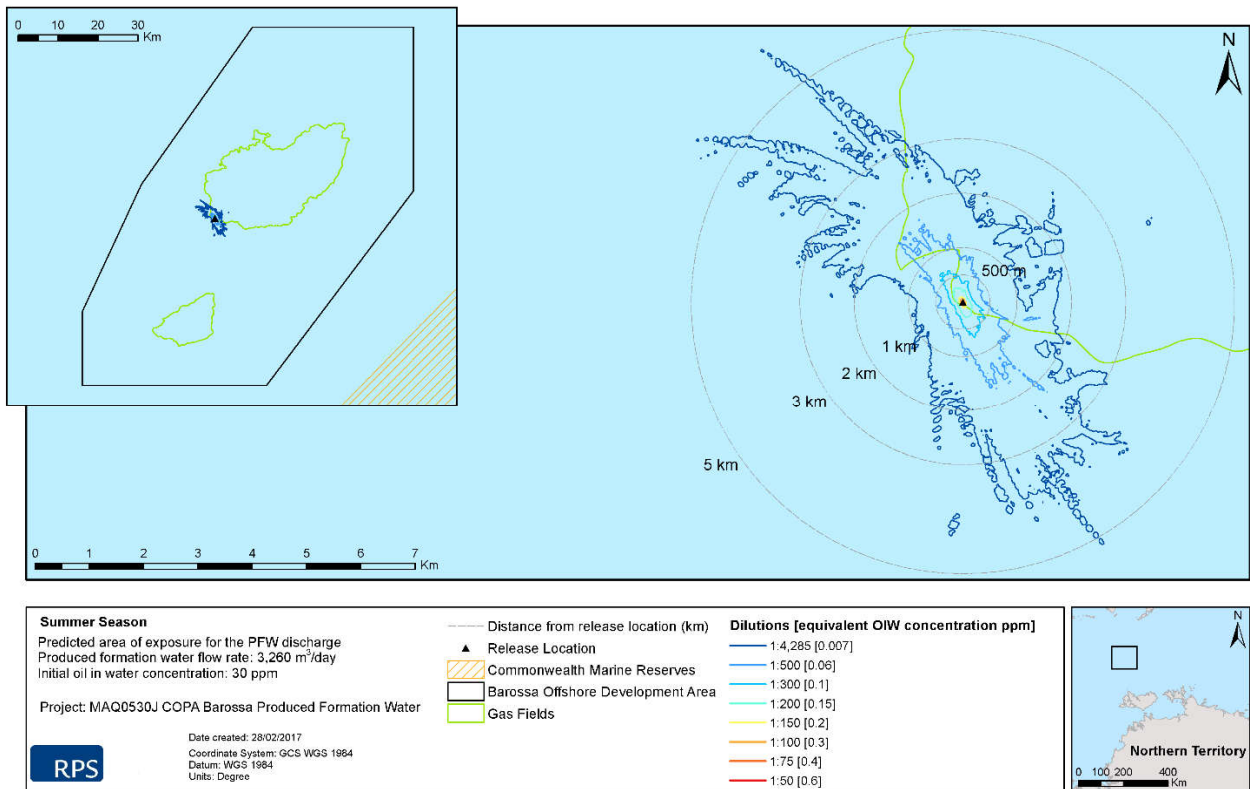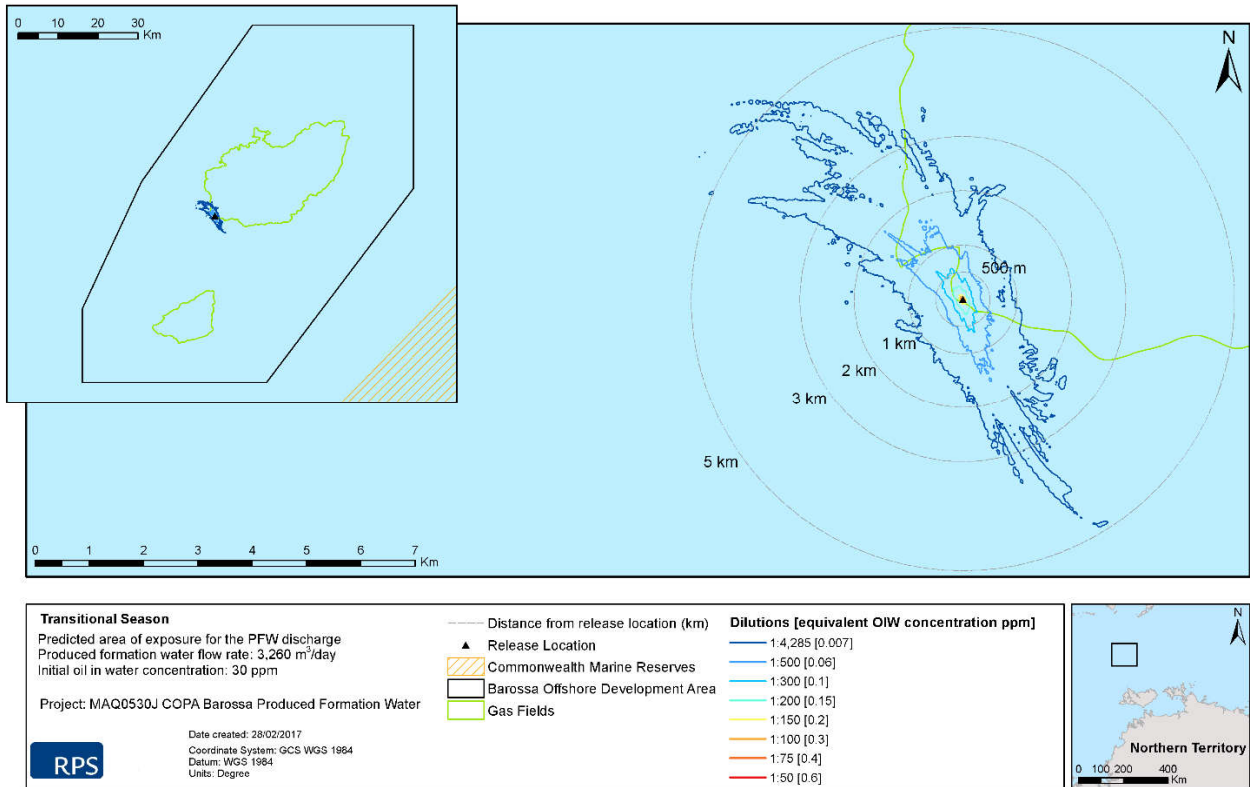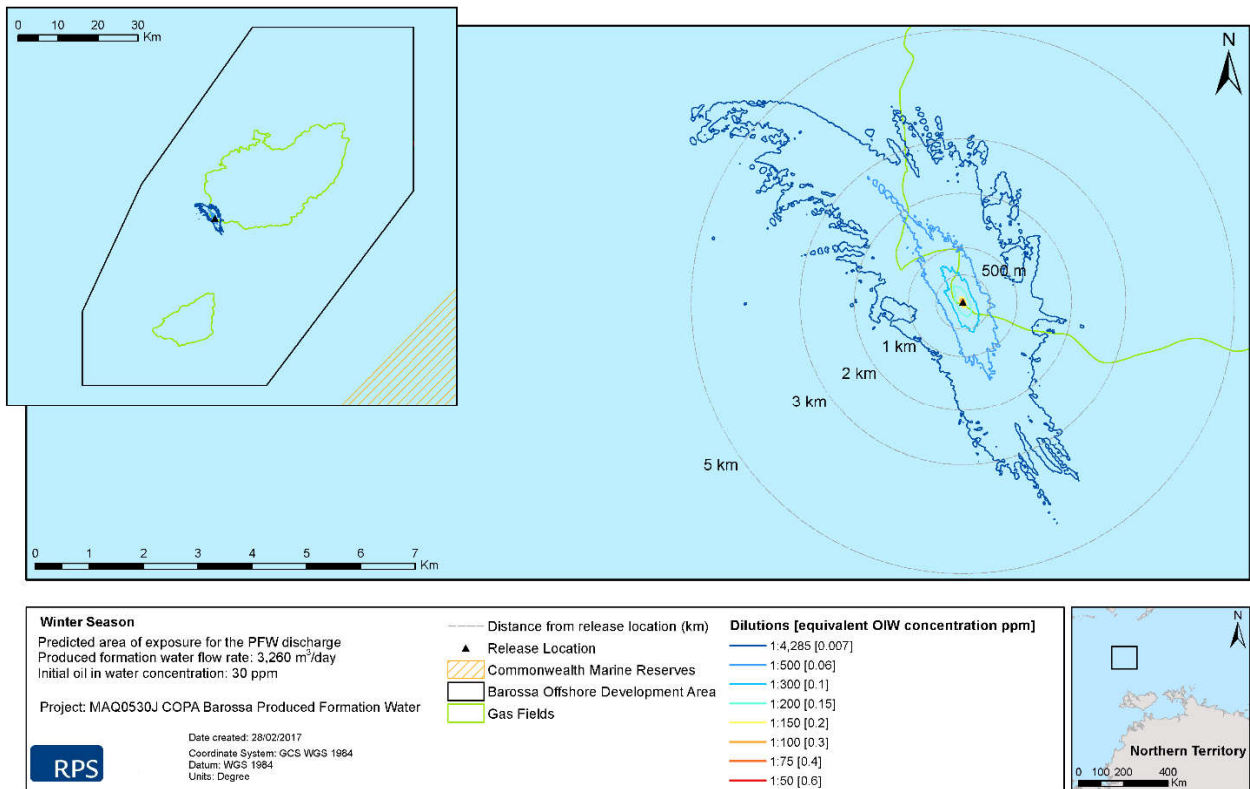

Figure 31 Predicted OIW dilutions under winter conditions for the maximum PFW flow rate (3,260 m³/d).

3.2.3 Combined analysis

Table 13 shows the maximum distance from release location to achieve a given dilution for each flow rate. The dilutions of 1:4,285 (equivalent to approximately 7 µg/L, which represents a 99% species protection level based on ANZECC/ARMCANZ (2000) guidelines) were predicted to be 4.57 km from the release location for the 1,590 m^3/d flow rate and 6.07 km for the 3,260 m^3/d flow rate. Based on distance from the 1:4,285 dilution contours to the nearest shoal/bank being Evans Shoal, no exposure is expected to non-transient species. However, pelagic species may come into contact with the plume and maybe exposed intermittently.

Table 14 shows the total area of coverage for a given dilution for each flow rate. Based on the 3,260 m^3/d flow rate and 1:4,285 dilution, the area of exposure was 12.39 km^2, which was approximately 53% larger than the mixing zone generated by the 1,590 m^3/d flow rate (8.11 km^2).

Figure 32 to Figure 33 present the predicted OIW dilutions based on combined results for 2010, 2012 and 2014 conditions for the minimum and maximum PFW flow rates, respectively.

Table 13 Maximum distance from PFW discharge release location to achieve a given dilution for each flow rate.

Flow rate (m³/d)	Maximum distance (km) from release location to achieve given dilution							
	1:50 dilution	1:75 dilution	1:100 dilution	1:150 dilution	1:200 dilution	1:300 dilution	1:500 dilution	1:4,285 dilution
1,590	<0.01	0.01	0.02	0.02	0.07	0.18	0.49	4.57
3,260	0.02	0.04	0.07	0.11	0.35	0.76	2.88	6.07

Table 14 Total area of coverage for a given dilution for each flow rate.

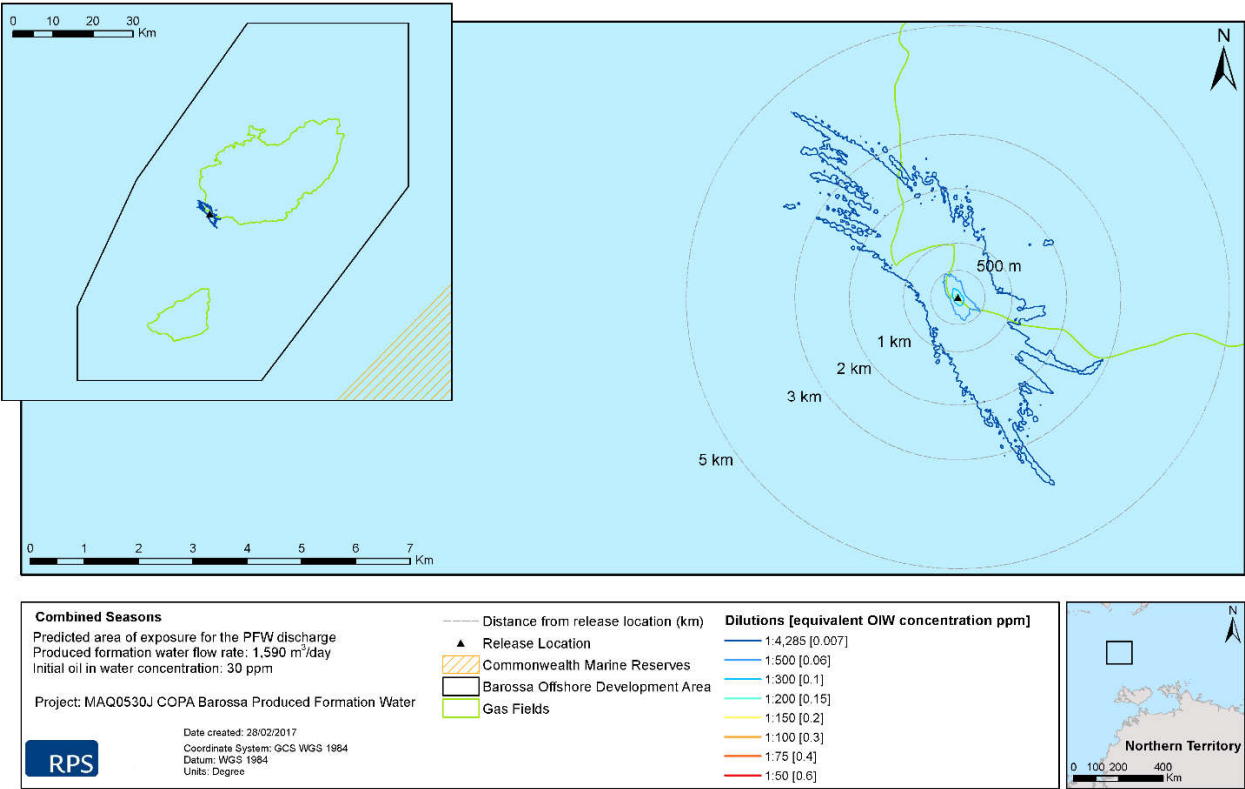| Flow rate (m³/d)	Total area (km²) of coverage for a given dilution							
	1:50 dilution	1:75 dilution	1:100 dilution	1:150 dilution	1:200 dilution	1:300 dilution	1:500 dilution	1:4,285 dilution
1,590	<0.001	<0.001	<0.001	<0.001	0.005	0.028	1.46	8.11
3,260	<0.001	<0.001	0.004	0.004	0.049	0.178	1.102	12.39

Figure 32 Predicted dilutions for the minimum PFW flow rate (1,590 m³/d).
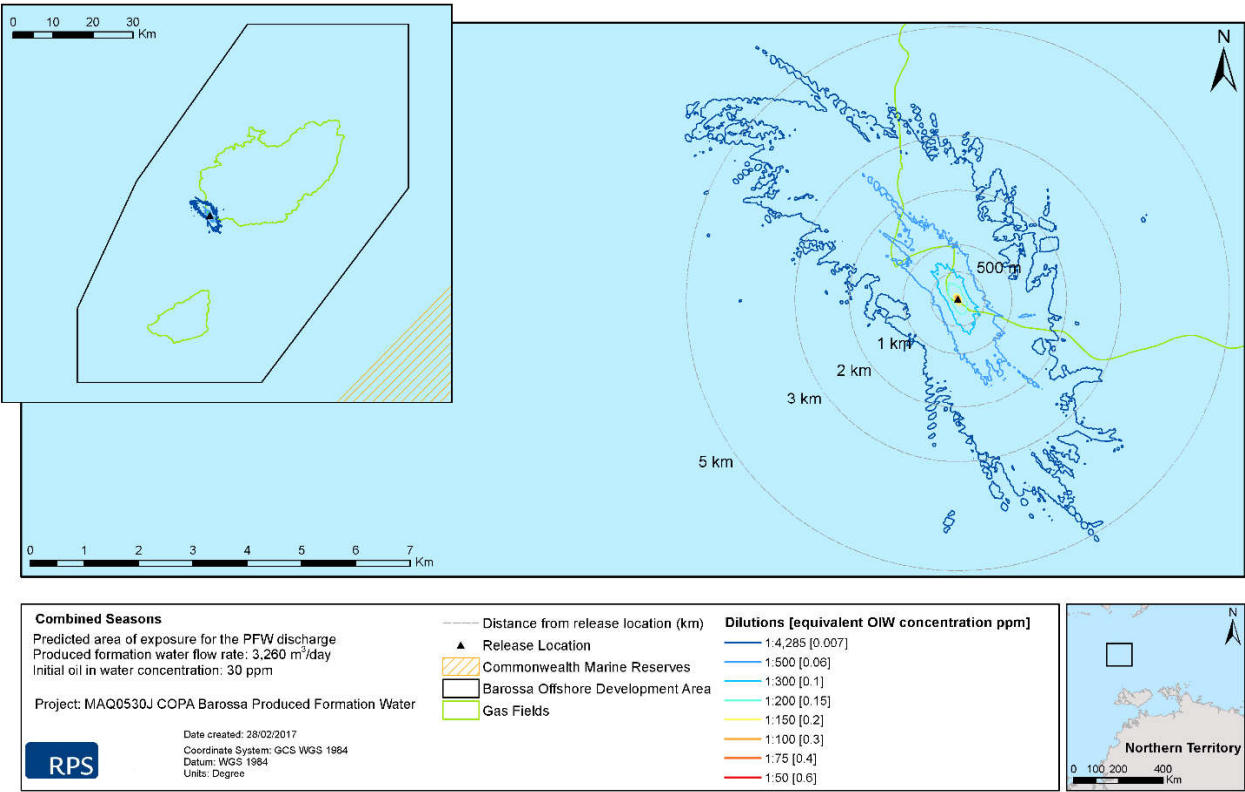

Figure 33 Predicted dilutions for the maximum PFW flow rate (3,260 m³/d).

4.0 References

Andersen, O.B. 1995. 'Global ocean tides from ERS 1 and TOPEX/POSEIDON altimetry'. Journal of Geophysical Research: Oceans, vol. 100, no. C12, pp. 25249–25259.

Australian Bureau of Meteorology. 2015. The Southern Oscillation Index – Monthly Southern Oscillation Index. viewed 28 September 2015, ftp://ftp.bom.gov.au/anon/home/ncc/www/sco/soi/soiplaintext.html.

Australian and New Zealand Environment and Conservation Council and Agricultural and Resource Management Council of Australia and New Zealand (ANZECC and ARMCANZ). 2000. Australian and New Zealand guidelines for fresh and marine water quality. Volume 1, The guidelines (National water quality management strategy; no.4). Australian and New Zealand Environment and Conservation Council and Agricultural and Resource Management Council of Australia and New Zealand, Canberra, Australian Capital Territory.

Baumgartner, D., Frick, W. and Roberts, P. 1994. Dilution models for Effluent Discharges, U.S. Environment Protection Agency, Newport.

Brandsma, M.G. and Sauer Jr, T.C. 1983a. 'The OOC Model: Prediction of Short Term fate of Drilling fluid in the Ocean. Part 1: Model Description'. Proceedings of MMS Workshop on An Evaluation of Effluent Dispersion and Fate Models for OCS Platforms. Minerals Management Service, Santa Barbara, California, pp. 58–84.

Brandsma, M.G. and Sauer Jr, T.C. 1983b. 'The OOC Model: Prediction of Short Term fate of Drilling fluid in the Ocean. Part 2: Model Results'. Proceedings of MMS Workshop on An Evaluation of Effluent Dispersion and Fate Models for OCS Platforms. Minerals Management Service, Santa Barbara, California, pp. 86-106.

Burns, K., Codi, S., Furnas, M., Heggie, D., Holdway, D., King, B. and McAllister, F. 1999. 'Dispersion and Fate of Produced Formation Water Constituents in an Australian Northwest Shelf Shallow Water Ecosystem'. Marine Pollution Bulletin, vol. 38, no. 7, pp. 593–603.

Carvalho, J.L.B., Roberts, P.J.W. and Roldão, J. 2002. 'Field Observations of the Ipanema Beach Outfall'. Journal of Hydraulic Engineering, vol. 128, no. 2, pp. 151–160.

Chassignet, E.P., Hurlburt, H.E., Smedstad, O.M., Halliwell, G.R., Hogan, P.J., Wallcraft, A.J., Baraille, R. and Bleck, R. 2007. 'The HYCOM (Hybrid Coordinate Ocean Model) data assimilative system'. Journal of Marine Systems, vol. 65, no. 1, pp. 60–83.

Chassignet, E., Hurlburt, H., Metzger, E., Smedstad, O., Cummings, J and Halliwell, G. 2009. 'U.S. GODAE: Global Ocean Prediction with the HYbrid Coordinate Ocean Model (HYCOM)'. Oceanography, vol. 22, no. 2, pp. 64–75.

Davies, A.M. 1977a. 'The numerical solutions of the three-dimensional hydrodynamic equations using a B-spline representation of the vertical current profile'. In: Nihoul, J.C. (ed). Bottom Turbulence: Proceedings of the 8th Liège Colloquium on Ocean Hydrodynamics, Elsevier Scientific, Amsterdam, pp. 1–25.

Davies, A.M. 1977b. 'Three-dimensional model with depth-varying eddy viscosity'. In: Nihoul, J.C. (ed), Bottom Turbulence: Proceedings of the 8th Liège Colloquium on Ocean Hydrodynamics, Elsevier Scientific, Amsterdam, pp. 27–48.

Frick, W.E., Roberts, P.J.W., Davis, L.R., Keyes, J., Baumgartner, D.J. and George, K.P. 2003. Dilution Models for Effluent Discharges (Visual Plumes) 4th Edition. Ecosystems Research Division U.S. Environmental Protection Agency, Georgia.

Fu, R., Del Genio, A.D. and Rossow, W.B. 1994. 'Influence of ocean surface conditions on atmospheric vertical thermodynamic structure and deep convection'. Journal of Climate, vol.7, no. 7, pp. 1092–1108.

Fugro. 2015. Barossa Field Meteorological, Current Profile, Wave and CTD Measurements – Final Report. Reporting Period: 8 July 2014 to 16 July 2015. Unpublished report prepared for ConocoPhillips Australia Pty Ltd., Perth, Western Australia.

Gordon, R. 1982. 'Wind driven circulation in Narragansett Bay' PhD thesis. Department of Ocean Engineering, University of Rhode Island.

International Finance Corporation World Bank Group (IFC). 2015. IFC's Sustainability Framework – Industry Sector Guidelines: Environmental, Health and Safety Guidelines For Offshore Oil And Gas Development. Available at: http://www.ifc.org/wps/wcm/connect/f3a7f38048cb251ea609b76bcf395ce1/FINAL_Jun+2015_Offshore+Oil+and+Gas_EHS+Guideline.pdf?MOD=AJPERES (accessed 22 February 2017).

Isaji, T. and Spaulding, M. 1984. 'A model of the tidally induced residual circulation in the Gulf of Maine and Georges Bank'. Journal of Physical Oceanography, vol. 14, no. 6, pp. 1119–1126.

Isaji, T., Howlett, E., Dalton C., and Anderson, E. 2001. 'Stepwise-continuous-variable-rectangular grid hydrodynamics model', Proceedings of the 24th Arctic and Marine Oil Spill Program (AMOP) Technical Seminar (including 18th TSOCS and 3rd PHYTO). Environment Canada, Edmonton, pp. 597–610.

Khondaker, A.N. 2000. 'Modeling the fate of drilling waste in marine environment – an overview'. Journal of Computers and Geosciences, vol. 26, no. 5, pp. 531–540.

King, B. and McAllister, F.A. 1997. 'The Application of MUDMAP to Investigate the Dilution and Mixing of the Above Water Discharge at the 'Harriet A' Petroleum Platform on the Northwest Shelf'. In: Modelling the Dispersion of Produced Water Discharge in Australia, Canberra, Australian Capital Territory.

King, B. and McAllister, F.A. 1998. 'Modelling the dispersion of produced water discharges', APPEA Journal, pp. 681–691.

Koh, R.C.Y. and Chang, Y.C. 1973. Mathematical model for barged ocean disposal of waste. United States Environmental Protection Agency, Washington.

Kostianoy, A.G., Ginzburg, A.I., Lebedev, S.A., Frankignoulle, M. and Delille, B. 2003. 'Fronts and mesoscale variability in the southern Indian Ocean as inferred from the TOPEX/POSEIDON and ERS-2 Altimetry data'. Oceanology, vol. 43, no. 5, pp. 632–642.

Ludicone, D., Santoleri, R., Marullo, S. and Gerosa, P. 1998. 'Sea level variability and surface eddy statistics in the Mediterranean Sea from TOPEX/POSEIDON data. Journal of Geophysical Research, vol. 103, no. C2, pp. 2995–3011.

Matsumoto, K., Takanezawa, T. and Ooe, M. 2000. 'Ocean tide models developed by assimilating TOPEX/POSEIDON altimeter data into hydrodynamical model: A global model and a regional model around Japan'. Journal of Oceanography, vol. 56, no.5, pp. 567–581.

National Aeronautics and Space Administration (NASA). 2013a. National Aeronautics and Space Administration/Jet Propulsion Laboratory TOPEX/Poseidon Fact Sheet. NASA. Available at: https://sealevel.jpl.nasa.gov/missions/topex/topexfactsheet (accessed 23 November 2013).

National Aeronautics and Space Administration (NASA). 2013b. National Aeronautics and Space Administration/Jet Propulsion Laboratory TOPEX/Poseidon. NASA. Available at: https://sealevel.jpl.nasa.gov/missions/topex (accessed 23 November 2013).

Owen, A. 1980. 'A three-dimensional model of the Bristol Channel'. Journal of Physical Oceanography, vol. 10, no. 8, pp. 1290–1302.

Philander, S.G. 1990. El Niño, La Niña, and the Southern Oscillation. Academic Press, San Diego.

Qiu, B. and Chen, S. 2010. 'Eddy-mean flow interaction in the decadally modulating Kuroshio Extension system'. Deep-Sea Research II, vol. 57, no. 13, 1098–1110.

Rasmusson, E.M. and Wallace, J.M. 1983. 'Meteorological aspects of the El Niño/southern oscillation'. Science, vol. 222, no. 4629, pp. 1195–1202.

Roberts, P. and Tian, X. 2004. 'New experimental techniques for validation of marine discharge models'. Environmental Modelling and Software, vol. 19, no. 7, pp. 691–699.

RPS Asia-Pacific Applied Science Associates (RPS APASA). 2015. Potential Barossa Development, Hydrodynamic Model Comparison with Field Measurements. Unpublished report prepared for ConocoPhillips Australia Pty Ltd., Perth, Western Australia.

Spaulding, M.L., Kolluru, V.S., Anderson, E. and Howlett, E. 1994. 'Application of three-dimensional oil spill model (WOSM/OILMAP) to hindcast the Braer Spill'. Spill Science and Technology Bulletin, vol. 1, no. 1, pp. 23–35.

Walstra, D.J.R., Van, Rijn, L.C., Blogg, H. and Van Ormondt, M. 2001. Evaluation of a hydrodynamic area model based on the COAST3D data at Teignmouth 1999. HR Wallingford, United Kingdom.

Woodside Energy Limited (Woodside). 2011. Browse LNG Development, Draft Upstream Environmental Impact Statement, EPBC Referral 2008/4111, November 2011.

Yaremchuk, M. and Tangdong, Q. 2004. 'Seasonal variability of the large-scale currents near the coast of the Philippines'. Journal of Physical Oceanography, vol. 34, no., 4, pp. 844–855.

Zigic, S., Zapata, M., Isaji,T., King, B. and Lemckert, C. 2003. 'Modelling of Moreton Bay using an ocean/coastal circulation model'. Proceedings of the 16th Australasian Coastal and Ocean Engineering Conference, the 9th Australasian Port and Harbour Conference and the Annual New Zealand Coastal Society Conference, Institution of Engineers Australia, Auckland, paper 170.

5.0 Appendices

5.1 Appendix A. Predicted plume temperature and distance plots for 1,590 m³/d flow rate

Figure 34 to Figure 36 illustrate the predicted difference in the PFW plume and ambient sea surface temperature versus distance from release location for the minimum flow rate (1,590 m³/d) under weak, medium and strong current strengths for 2010, 2012 and 2014 seasonal conditions.
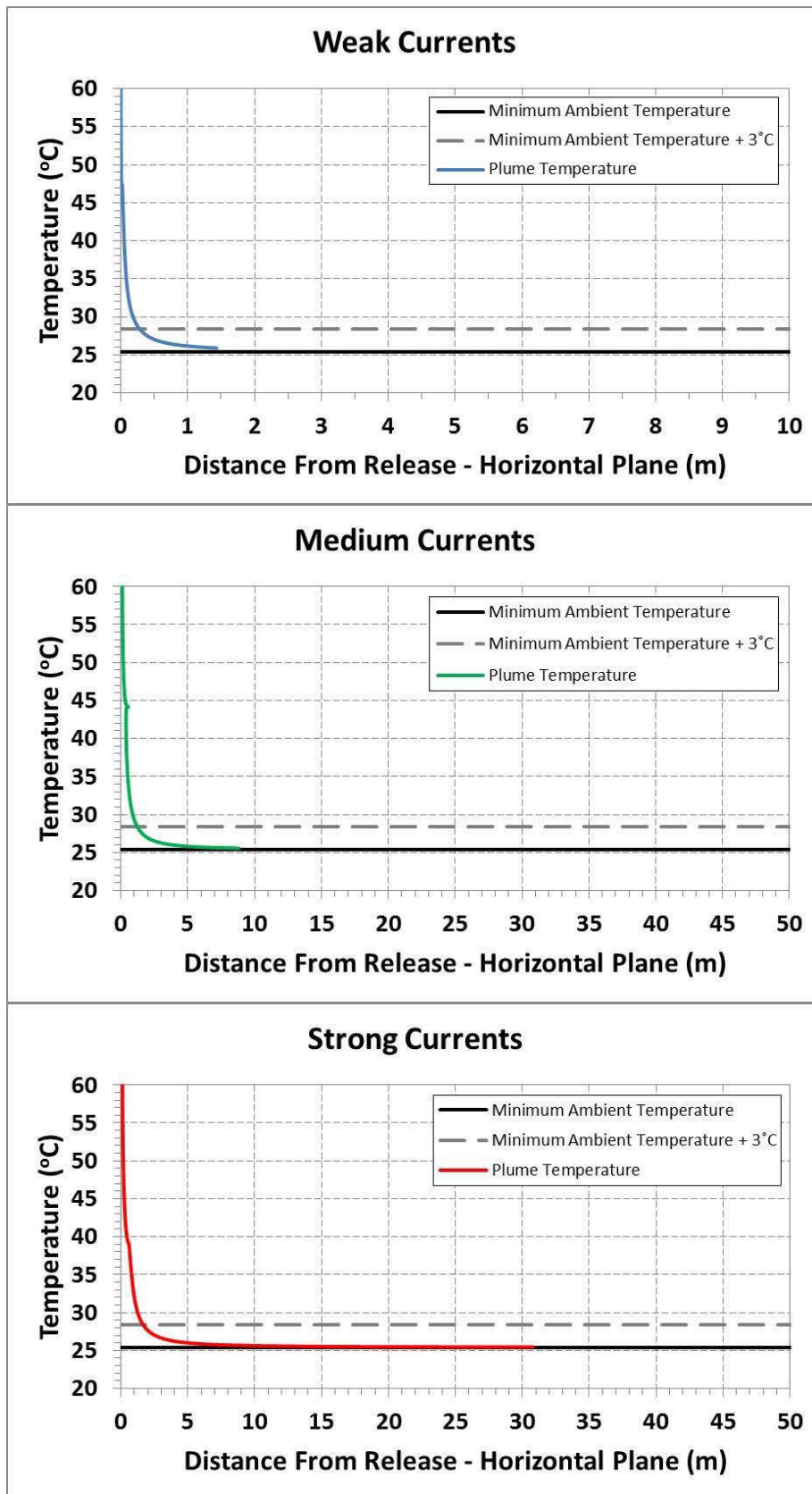
Figure 34 Predicted change in PFW plume temperature as a function of distance from release location under weak, medium and strong current strengths during summer conditions (1,590 m³/d)
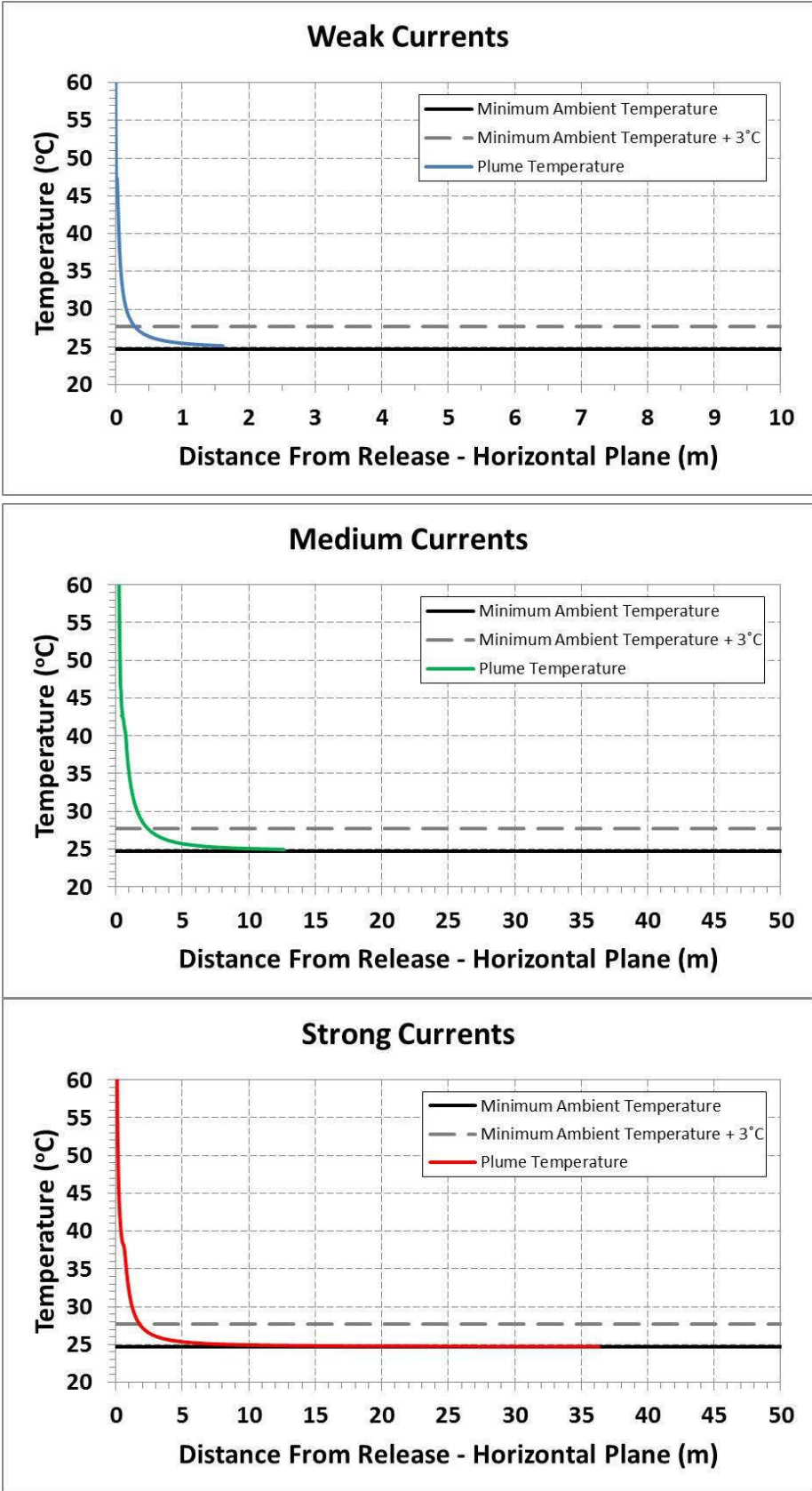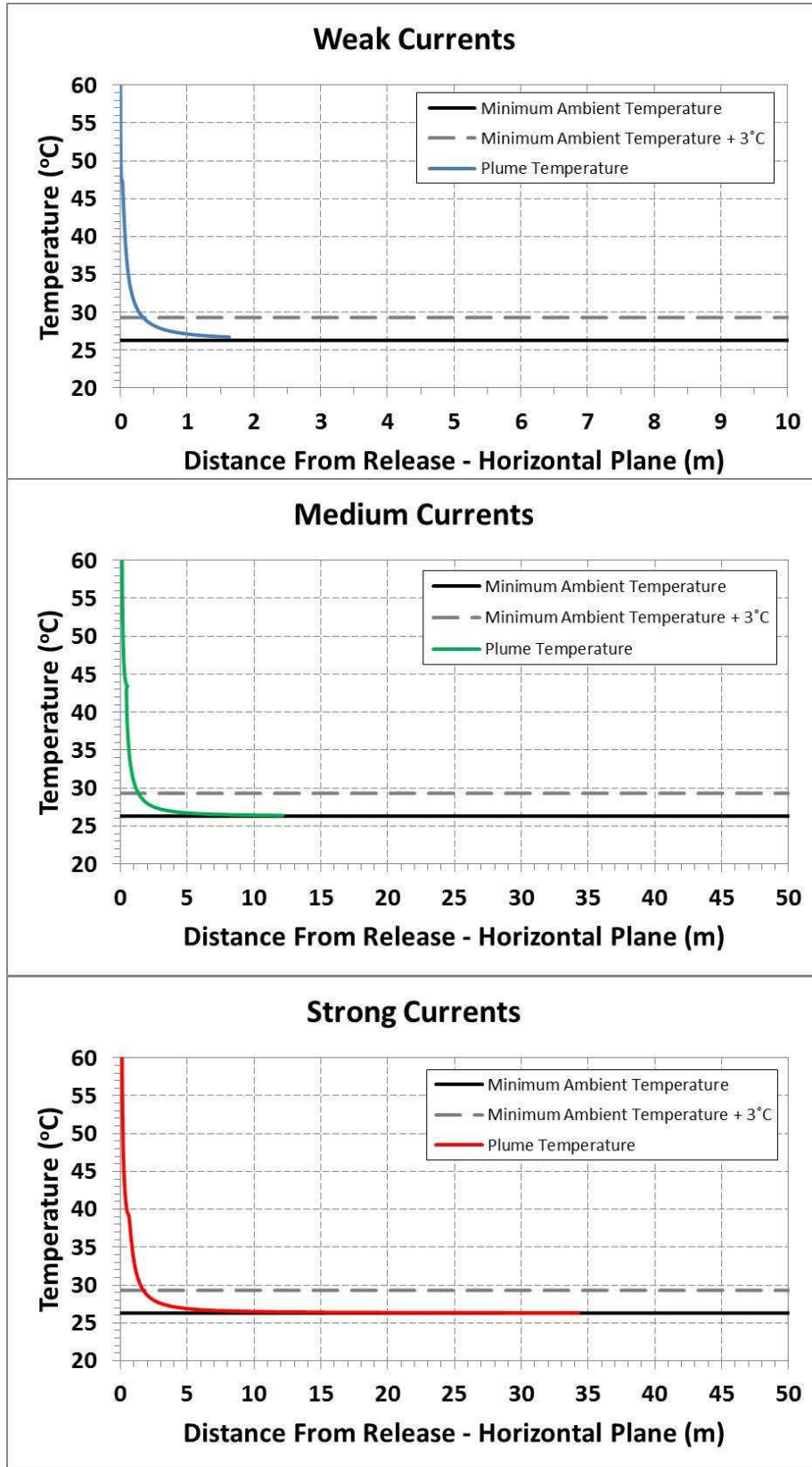
Figure 35 Predicted change in PFW plume temperature as a function of distance from release location under weak, medium and strong current strengths during transitional conditions (1,590 m^3/d)

Figure 36 Predicted change in PFW plume temperature as a function of distance from release location under weak, medium and strong current strengths during winter conditions (1,590 m³/d)

5.2 Appendix B. Predicted plume temperature and distance plots for 3,260 m³/d flow rate

Figure 37 to Figure 39 illustrate the predicted difference in PFW plume and ambient sea surface temperature versus distance from release location for the maximum flow rate (3,260 m³/d) under weak, medium and strong current strengths for 2010, 2012 and 2014 seasonal conditions.
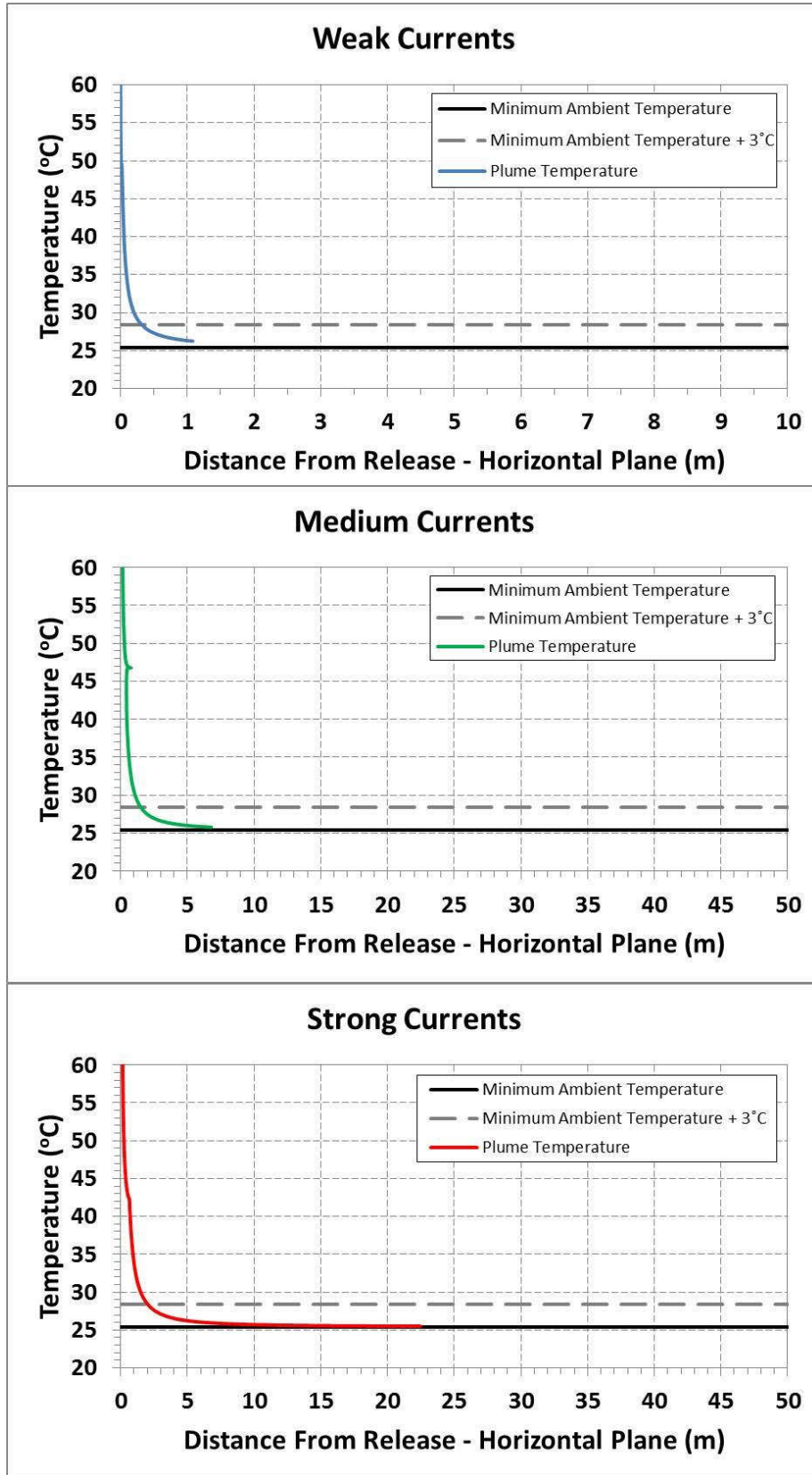
Figure 37 Predicted change in PFW plume temperature as a function of distance from release location under weak, medium and strong current strengths during summer conditions (3,260 m³/d)
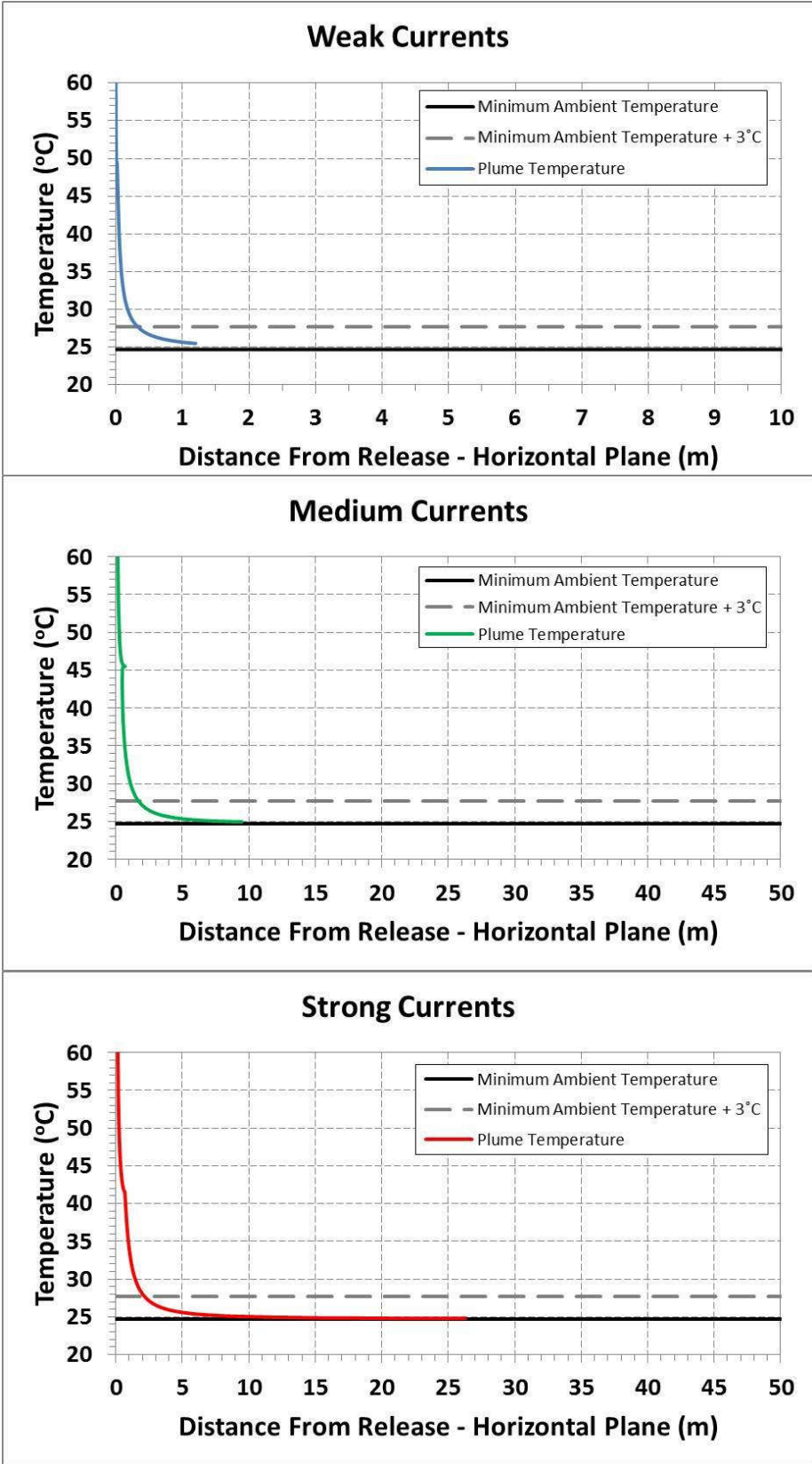
Figure 38 Predicted change in PFW plume temperature as a function of distance from release location under weak, medium and strong current strengths during transitional conditions (3,260 m^3/d)
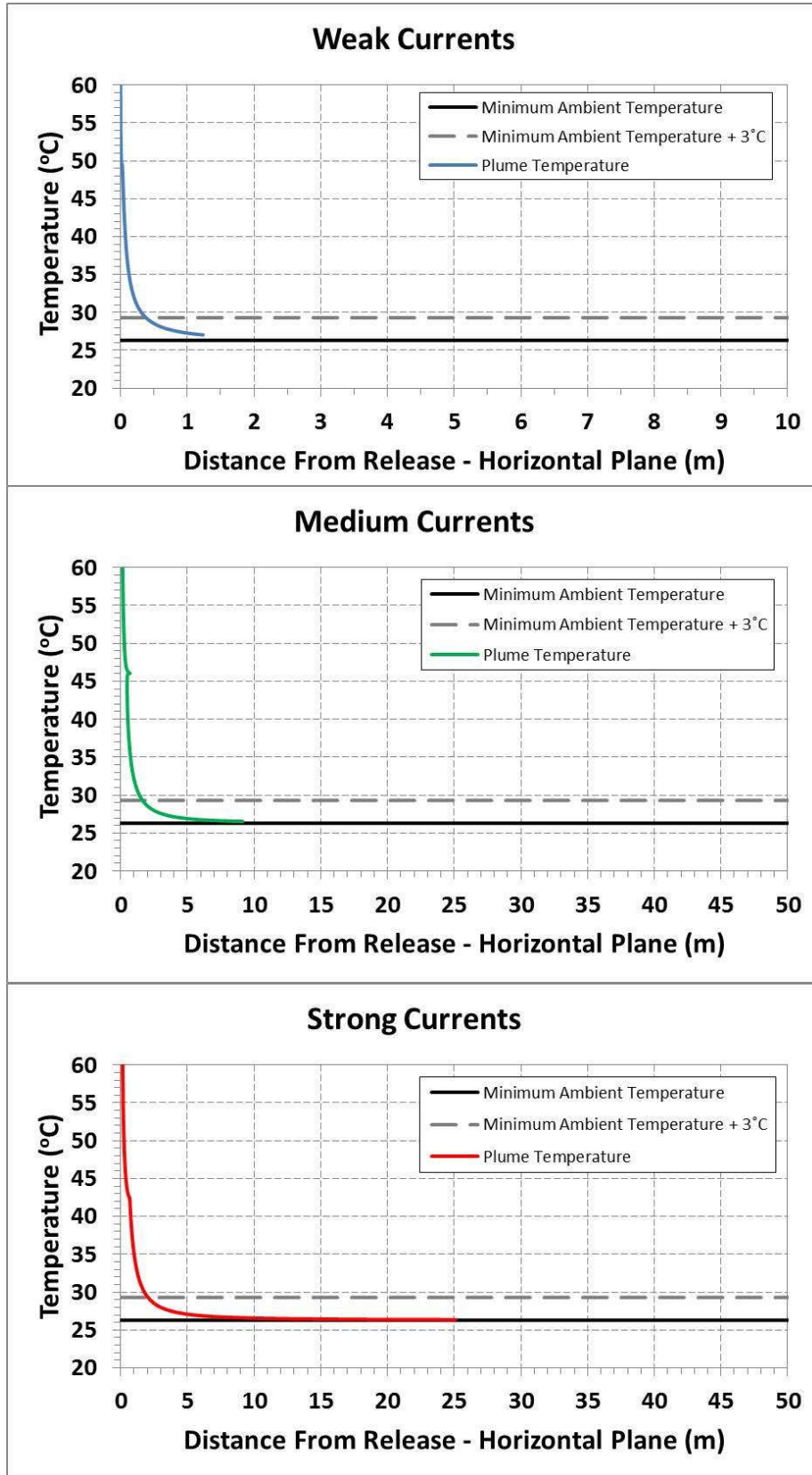
Figure 39 Predicted change in PFW plume temperature as a function of distance from release location under weak, medium and strong current strengths during winter conditions (3,260 m³/d)